

Received 22 November 2023, accepted 14 December 2023, date of publication 25 December 2023, date of current version 29 December 2023.

Digital Object Identifier 10.1109/ACCESS.2023.3346433

RESEARCH ARTICLE

A New Strategy for Combining Nonlinear Kalman Filters With Smooth Variable Structure Filters

SALMAN AKHTAR¹, **PEYMAN SETOODEH**¹, (Senior Member, IEEE),
RYAN AHMED, AND **SAEID HABIBI**, (Member, IEEE)

Department of Mechanical Engineering, McMaster University, Hamilton, ON L8S 4L8, Canada

Corresponding author: Salman Akhtar (akhtarsm@mcmaster.ca)

This work was supported in part by the Federal Economic Development Agency for Southern Ontario (FedDev) under Grant 814996 and in part by Ontario Research Fund Research Excellence (ORF) under Grant 08-044.

ABSTRACT Bayesian filters exemplified by the celebrated Kalman Filter (KF), and its non-linear variants rely on a fairly accurate state-space model of the system under study. To address the issue of modelling uncertainty in state estimation, the Smooth Variable Structure Filter (SVSF) was proposed in 2007. Since then, several SVSF variants have been proposed to extend its domain of applicability. In some of these algorithms, SVSF has been viewed as a complementary approach alongside the well-established nonlinear Kalman Filters. This paper seeks a general framework for SVSF formulation to unify some of the recent developments in SVSF literature under one umbrella. In this way, the SVSF variants are revisited as special cases of the proposed framework. This paper proposes a new strategy to combine SVSF filters with other nonlinear filters and puts existing SVSF filters under one umbrella. Six filters are formulated based on the proposed method of combining filters. The proposed filters relax limitations of existing SVSF variants, making the proposed filters more universal. In simulations, the new filters outperform state-of-the-art nonlinear KFs and some existing SVSF filters. To demonstrate the merits of the proposed framework, the new filters are applied to target tracking and are comparatively evaluated.

INDEX TERMS Target tracking, state estimation, estimation theory, smooth variable structure filter, Kalman filters, variable structure systems, maneuvering targets.

I. INTRODUCTION

The general formulation of Bayesian optimal filtering leads to a conceptual solution, which is computationally intractable, except for the special case of the Kalman Filter (KF) [1]. The KF is optimal in terms of minimum mean squared error (MMSE) subject to the system being linear and the noise being Gaussian with known statistics [2], [3], [4]. However, in reality, many systems are non-linear with scented noise distributions. To handle non-linear systems, there are two main approaches to approximate the conceptual Bayesian solution and obtain suboptimal filters [5]:

- Approximating the non-linear functions in the state and measurement equations of the state-space model using a power series: The Extended Kalman Filter (EKF) and Divided Difference Filter (DDF) are derived in this way [3], [5]. In the EKF, linearization is applied to

the system and/or measurement models by applying a Taylor Series approximation, and the resulting Jacobian matrices are used to approximate the state covariance matrix. However, one issue with this strategy is that if the system is highly non-linear, the filter may become unstable or its performance may degrade. Moreover, obtaining Jacobian matrices may be difficult depending on the application at hand.

- Approximating the probability distributions using a set of sample points: the Unscented Kalman Filter (UKF), Cubature Kalman Filter (CKF), and Particle Filter (PF) follow this approach [5]. In the UKF, a deterministic sampling technique, known as the Unscented Transformation (UT) is used to approximate probability distributions [6], where for the input distribution of the functions, sigma points are selected based on the corresponding mean and covariance. These points are then propagated through the non-linear system and/or measurement models to approximate the mean and

The associate editor coordinating the review of this manuscript and approving it for publication was Ángel F. García-Fernández¹.

covariance of the output distributions. This technique is accurate with up to a 3rd-order series expansion [7].

In practice, it is difficult to obtain perfect models for systems. For instance, in target tracking, which can be viewed as a challenging application of filters, obtaining accurate models is difficult, especially when the target maneuvers. Target-tracking is utilized in tasks such as situational awareness, environmental sensing and interpretation, and safety. Tracking is the process of estimating the state of a remote moving object using uncertain, inaccurate, and indirect measurements from one or multiple sensors [4], [8]. It has been applied to a number of areas, including military and surveillance [4], [8], [9], medical imaging [10], robotics [11], and autonomous vehicles [12], [13], [14]. Sensors commonly used to detect objects and obtain measurements are radar [9], [12], LIDAR [13], and vision camera [14]. These measurements are then fed into a tracker to estimate states of moving targets such as position, velocity, and acceleration. In the context of target tracking, targets tend to maneuver as they move. For example, in traffic monitoring and autonomous driving applications, vehicle targets exhibit several types of maneuvers such as lane-changes, accelerations, and turns. Since obtaining an accurate dynamic model for the motion of a maneuvering target is challenging, the states of such a target must be robustly estimated. Therefore, robust and accurate state estimates are critical for the design of target-tracking systems. Robust state estimation refers to a category of filtering techniques that are used to compensate for inaccurate modelling. These filters have the ability to perform estimation under the presence of modelling uncertainties and can handle a larger range of modelling errors compared to conventional KF-based techniques. Examples of robust state estimation methods include the Robust Kalman Filter [15], H-infinity Filter [16], and Smooth Variable Structure Filter (SVSF) [17].

The SVSF follows a predictor-corrector form likewise to the KF. The technique is formulated based on Sliding Mode Control (SMC), where the state estimate is forced to converge to a region around the true trajectory of the system. In the SVSF, a switching gain is applied in order to keep the state estimate moving back and forth across the true state trajectory. As such, it benefits from the stability features of SMC, and it is shown to be robust against modelling uncertainties [17]. The SVSF is a robust state and parameter estimation strategy that can guarantee numerical stability and can recover its performance in the presence of a fault condition. It allows for the explicit definition of the source of uncertainty and can guarantee stability given an upper bound for uncertainties and disturbances. The SVSF has demonstrated robust performance in several applications, including Artificial Neural Network training [18], battery state of charge estimation [19], electric power grids [20], fault detection and diagnosis [21], target tracking [22], robot localization and mapping [23], robot manipulators [24], satellite state estimation [25], and trajectory prediction for autonomous driving [26].

Many advancements have been proposed for the SVSF, with an overview given in [27]. The initial formulation provided in [17] has no state covariance formulation. It was followed by a revised version with a covariance as reported in [28]. In [29], an optimal smoothing variable boundary layer (VBL) was formed for the SVSF by minimizing the trace of the a posteriori covariance matrix; this approach is called the VBL-SVSF. In [30], [31], and [32], the SVSF was combined with the EKF, UKF, CKF, and PF. These extended formulations combine the advantages of these different filters with robustness of the SVSF. The Interacting Multiple Model (IMM) estimator was combined with the SVSF in [33]. In the more general formulations of the SVSF reported in [17] and [34], where the number of measured states is less than the number of states, the filters are derived for linear systems by incorporating a reduced-order Luenberger observer. In [34], a covariance matrix was derived for this filter and was then applied to track targets in the presence of clutter by combining it with Probabilistic Data Association (PDA) and Joint Probabilistic Data Association (JPDA) methods. This work was further extended to formulate an optimal smoothing variable boundary layer for the filter in [34], called Generalized Variable Boundary Layer - Smooth Variable Structure Filter (GVBL-SVSF), which was obtained through minimizing the trace of the SVSF state covariance in [34]. This method was also combined with JPDA to track targets for automotive applications using LIDAR data. Other formulations of the SVSF include the Square-root SVSF [35], 2nd-order SVSF [36], Predictive SVSF [25], Hyperbolic Tangent SVSF (Tanh-SVSF) [37], and Non-linear Variable Boundary Layer SVSF (NVBL-SVSF) [38].

It is worth noting the following points regarding the contributions of this paper. Table 1 summarizes the recent advances in SVSF literature along with the limitations of each algorithm. This paper aims at developing a general framework for the SVSF formulation. To be more precise, a new strategy for combining SVSF with other popular nonlinear filters is proposed. This results in a set of filters, where each one combines SVSF with a state-of-the-art nonlinear filter. The mentioned algorithms in Table 1 can be subsumed under the proposed set of filters. In other words, all SVSF filters in that table can be discovered as special cases of the proposed filters. Thus, a key contribution of this paper is that the framework puts all these filters under one umbrella. Furthermore, Table 1 shows how the proposed set of filters relax limitations of existing SVSF strategies. Another key contribution of this work is that the proposed filters relax limitations of all SVSF filters in Table 1, which makes the proposed strategies more universal than the ones mentioned in the table. Through relaxing these limitations, the proposed approaches contain features that not all filters in Table 1 have. In summary, as stated in Table 1, the relaxed limitations include:

- No covariance matrix for some SVSF filters, which is needed in a multi-target tracking pipeline for tasks such as data association as specified in [8]. Moreover, the

IMM algorithm can be used in conjunction with the proposed filters as they provide a covariance matrix.

- Requirement of a full measurement matrix. The proposed framework relaxes the requirement of measuring all states, which is not always possible in practice. Adding more sensors to obtain more measurements increases the system cost. Although artificial measurements can be derived to create a measurement for unmeasured states, they may introduce additional noise and for some states it may be impossible to obtain an artificial measurement.
- The GVBL-SVSF and NVBL-SVSF were derived and applied to linear systems. The proposed framework in this paper extends the domain of applicability of the GVBL-SVSF and NVBL-SVSF to systems with non-linear dynamic models.
- Not all SVSF-based filters take advantage of KF-based filtering, which is beneficial when the modelling error is low.

The performance of these proposed combined filters resulting from the proposed framework are evaluated in a maneuvering target scenario. It is shown that the proposed algorithms outperform the conventional EKF, UKF, and CKF estimators as well as five selected existing non-linear SVSF strategies.

The rest of the paper is organized as follows. Section II presents the proposed framework that is formed such that existing SVSF strategies are put under one umbrella. The derivations and algorithms for the proposed combined filters are presented in that section. Simulation results are shown in Section III, where a simulated maneuvering target scenario is used for comparative performance evaluation. Section IV concludes the paper.

II. PROPOSED STRATEGY TO COMBINE FILTERS

In the proposed framework, a new approach for combining SVSF with other non-linear filters is developed. This results in a set of six combined filters, where for three, the Luenberger SVSF (SVSF-L) is combined with EKF, UKF, and CKF. For the other three, the Luenberger Hyperbolic Tangent SVSF (Tanh-SVSF-L) is combined also with EKF, UKF, and CKF. This framework puts all SVSF filters in Table 1 under one umbrella because these filters can be discovered as special cases of the proposed filters. Moreover, all limitations stated in Table 1 are relaxed by the proposed filters. This section provides a detailed derivation of the proposed filtering algorithms. The derivations of all filters build on the presented algorithms in [22], [30], [31], and [38], but relax some of their limiting assumptions:

- In [30] and [31], three SVSF variants were presented that deploy EKF, UKF, and CKF. Furthermore, they rely on the VBL-SVSF from [29] to compute variable boundary layer widths through minimizing the trace of the a posteriori covariance matrix of the SVSF in [29]. The VBL in other words is used as a method to combine SVSF with nonlinear KFs (EKF, UKF,

and CKF). These calculated boundary layer widths obtained from the VBL are then compared to user-defined thresholds. If the boundary layer widths are below the thresholds, then the EKF/UKF/CKF gain will be applied, otherwise, the SVSF gain will be used to preserve the technique's robustness against modelling uncertainty. In the case when the measurement model is linear and the system model is nonlinear, these approaches are applicable to non-linear systems with the same number of states and outputs (measured states), $n = m$, where m denotes the number of measured states and n is the total number of states. Although artificial measurements can be generated for cases with $m < n$, this makes the technique to some extent more heuristic. Also, it is not always possible to obtain artificial measurements of unmeasured states. Adding more sensors to measure more states may increase system cost too. This constraint on the number of measurements is relaxed by the proposed framework of this paper, which makes it more suitable for target-tracking, where typically $m < n$.

- In [22] and [38], the GVBL-SVSF and NVBL-SVSF were established for linear systems, in which the number of outputs (measured states) is less than the number of states, $m < n$. Both apply a similar approach to VBL-SVSF in [29], but the difference is that both compute the optimal boundary layer widths separately for the measured and unmeasured states. The optimal widths are then compared to thresholds, if they are below the thresholds, the ordinary KF gain is used, otherwise, the corresponding SVSF (SVSF-L or Tanh-SVSF-L) gain is deployed. A limitation of GVBL-SVSF and NVBL-SVSF is that they are applied to systems with a linear system model. This linearity constraint is relaxed by the proposed framework of this paper.

In the proposed framework in this paper, the GVBL-SVSF and NVBL-SVSF are extended to non-linear systems in multiple forms in combination with the EKF, UKF, and CKF estimators, where the number of measured states is lower than the number of states, $m < n$. More specifically, in this framework, a new strategy is proposed to combine SVSF with nonlinear KFs. Figure 1 shows a flowchart of how the strategy works. In summary, after state prediction executes, this method uses a variable boundary layer, either the Generalized Variable Boundary Layer (GVBL) in [22] or the Non-linear Variable Boundary Layer (NVBL) in [38] to obtain boundary layer (BL) widths separately for measured and unmeasured states. The widths are compared to thresholds to determine whether to apply the SVSF (SVSF-L or Tanh-SVSF-L) gain or a KF-based filter gain (EKF, UKF, or CKF). Afterwards, the measured and unmeasured states are updated separately. This results in a set of six combined filters, namely, EK-SVSF-L, UK-SVSF-L, CK-SVSF-L, EK-Tanh-SVSF-L, UK-Tanh-SVSF-L, and CK-Tanh-SVSF-L. The limitations of SVSF filters in Table 1 are relaxed and these filters can be discovered as special cases of the proposed filters, allowing

TABLE 1. SVSF strategies that are special cases of the proposed framework.

Filter Name and Abbreviation	Limitations	How the Limitations are Relaxed by the Proposed Filters	References
Initial SVSF (SVSF-I)	No covariance	Builds on SVSF strategies with a covariance	[17]
Luenberger SVSF (SVSF-L)	No covariance	Builds on SVSF strategies with a covariance	[17]
Initial SVSF with a covariance (C-SVSF-I)	Requires all states to be measured	Extends SVSF filters with a non-square measurement matrix	[28]
Variable Boundary Layer-SVSF (VBL-SVSF)	Requires all states to be measured	Extends SVSF filters with a non-square measurement matrix	[29]
Initial Extended Kalman – SVSF (EK-SVSF-I)	Requires all states to be measured	Replaces the KF modules of the GVBL-SVSF with the EKF	[31]
Initial Unscented Kalman – SVSF (UK-SVSF-I)	Requires all states to be measured	Replaces the KF modules of the GVBL-SVSF with the UKF	[31]
Initial Cubature Kalman – SVSF (CK-SVSF-I)	Requires all states to be measured	Replaces the KF modules of the GVBL-SVSF with the CKF	[30]
Luenberger SVSF with a covariance (C-SVSF-L)	Does not take advantage of other filters when the level of modelling error is low	Builds on a filter that combines advantages of the KF and C-SVSF-L, which is the GVBL-SVSF	[34]
Generalized Variable Boundary Layer – SVSF (GVBL-SVSF)	Defined for linear systems	Extends this strategy to non-linear systems from replacing the KF modules of the GVBL-SVSF with a nonlinear filter (EKF, UKF, CKF)	[22]
Initial Hyperbolic Tangent – SVSF (Tanh-SVSF-I)	Requires all states to be measured	Builds on the Luenberger Tanh-SVSF, which is formulated for systems with fewer measured states	[37]
Luenberger Hyperbolic Tangent – SVSF (Tanh-SVSF-L)	Does not take advantage of other filters when the level of modelling error is low	Builds on a filter that combines advantages of the KF with Tanh-SVSF-L, which is NVBL-SVSF	[37]
Nonlinear Variable Boundary Layer – SVSF (NVBL-SVSF)	Defined for linear systems	Replaces the KF modules of NVBL-SVSF with a non-linear filter (EKF, UKF, CKF)	[38]

the proposed framework to put existing filters under one umbrella. The filters are derived in the following subsections.

A. SMOOTH VARIABLE STRUCTURE FILTER (SVSF)

Before presenting the proposed strategies, a general overview of how the SVSF works is presented. Similar to the KF, it has a predictor-corrector formulation. The main difference is that the gain derivation and the filter are developed based on the sliding mode concept [17]. Through this, the filter gain is computed such that the estimated state converges to a region around the true state trajectory as shown in Figure 2. This region is known as the existence subspace and the width of this region, denoted by β , is dependent on the level of modelling uncertainties as well as disturbances [17]. Within this subspace, the estimated state follows a zig-zag pattern in Figure 2b, which is due to the discontinuous corrective action from the switching gain. In other words, the gain forces the estimated state trajectory to move back and forth across the system state trajectory (true trajectory). This state estimator is proven to be stable and robust to modelling errors as well as disturbances if there exists an upper bound on the level of modelling uncertainties [17]. The zig-zag pattern due to the discontinuous corrective action is known as chattering, which is undesirable, and this results from measurement noise, modelling errors, and disturbances. One method to suppress chattering is utilize a smoothing boundary layer (BL) denoted by ψ [17]. From applying the BL, the gain's corrective action in a region surrounding the switching hyperplane, called the neighborhood (denoted by ψ), is linearly interpolated to smoothen the estimated trajectory [17]. Figure 2 illustrates

the concept. In Figure 2a, chattering is smoothened if the smoothing boundary layer width is larger than the width of the existence subspace, whereas in Figure 2b, chattering is present when the smoothing subspace width is smaller.

For all of the proposed filters, the system and measurement models follow this form:

$$\mathbf{x}_{k+1} = \mathbf{f}(\mathbf{x}_k, \mathbf{u}_k) + \mathbf{v}_k \quad (1)$$

$$\mathbf{z}_k = \mathbf{H}_k \mathbf{x}_k + \mathbf{w}_k \quad (2)$$

where \mathbf{x}_k is the state vector, which is of dimensions $n \times 1$, \mathbf{z}_k is the measurement vector with dimensions $m \times 1$, and \mathbf{u}_k is the control vector, which is of dimensions $p \times 1$, where p is the number of control inputs. $\mathbf{f}(\mathbf{x}_k, \mathbf{u}_k)$ is the nonlinear state transition function, which outputs an $n \times 1$ vector and \mathbf{H}_k is the measurement matrix with dimensions $m \times n$. \mathbf{v}_k and \mathbf{w}_k are process and measurement noise vectors, respectively. The respective dimensions of these vectors are $n \times 1$ and $m \times 1$, where \mathbf{v}_k is white Gaussian noise that is zero-mean with covariance \mathbf{Q}_k , and \mathbf{w}_k is zero-mean Gaussian noise with covariance \mathbf{R}_k . The process and measurement noise vectors are assumed to be mutually independent of each other.

B. PROPOSED STRATEGY TO COMBINE FILTERS

The derivations for each combined filter are shown in the following subsections. Each filter follows the flowchart shown in Figure 1, where state prediction executes first and then depending on whether the combination is with the SVSF-L or Tanh-SVSF-L, either the GVBL or NVBL is computed. If the filter combines SVSF-L with a nonlinear

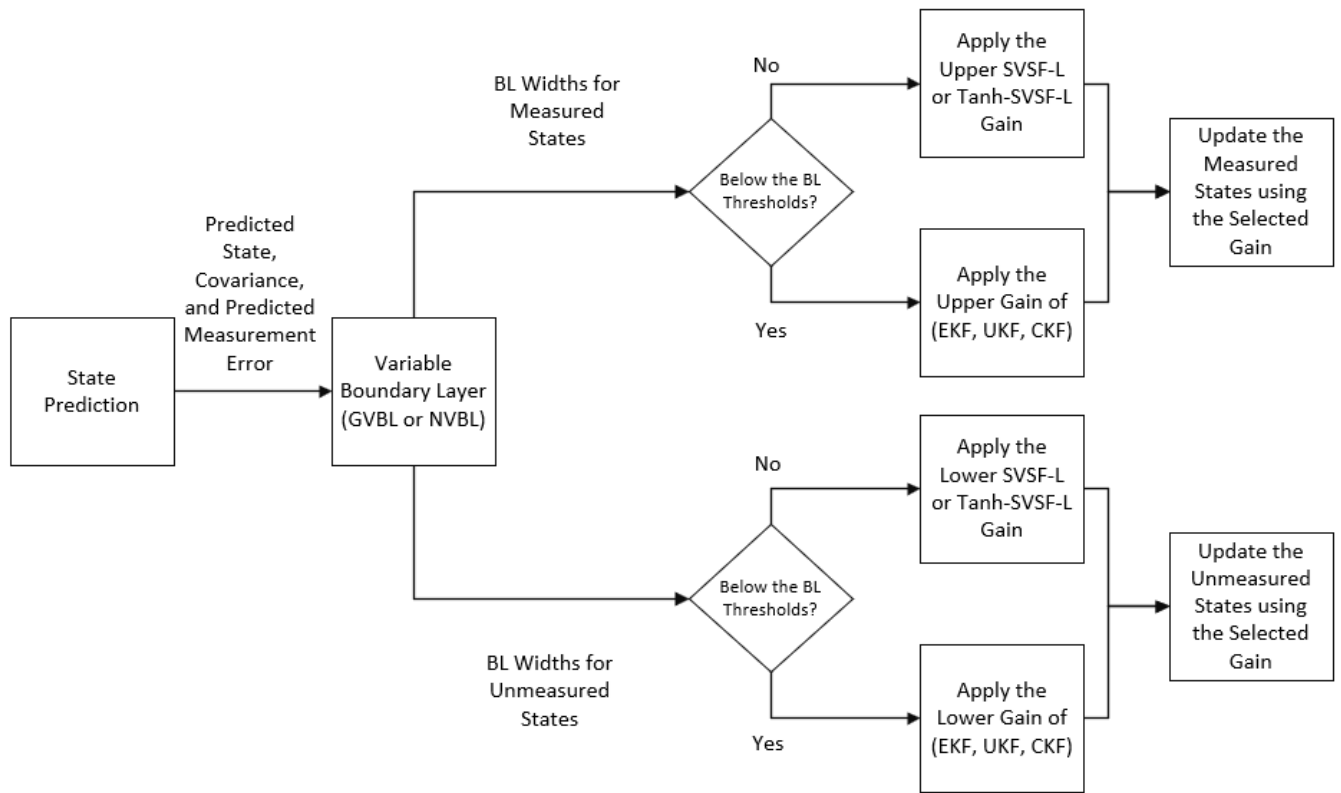


FIGURE 1. The proposed framework/methodology to combine SVSF with nonlinear KF-based filters.

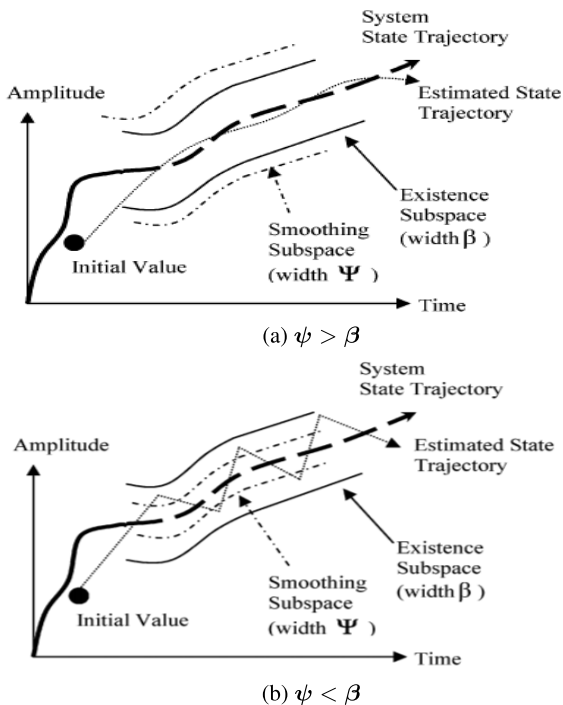


FIGURE 2. Effects of varying the boundary layer width [17].

KF, then GVBL is used. If the filter combines Tanh-SVSF-L with EKF/UKF/CKF, then the NVBL is calculated. Both

VBLs output the BL widths for the measured and unmeasured states. The BL widths quantify the level of modelling error for each state. First, the BL widths for the measured states are compared to thresholds to select the gain to correct the measured state estimates. If the BL width of any measured state is above its user-defined threshold, then an upper SVSF gain is used to take advantage of robustness and stability. SVSF is more advantageous when there are higher levels of modelling error. If GVBL is used, the upper SVSF-L gain is applied. Otherwise, if NVBL is used, the upper Tanh-SVSF-L gain is utilized. If all BL widths are below their respective thresholds, then the upper gain of the EKF, UKF, or CKF is used to correct the measured state estimates because nonlinear KFs are advantageous when the level of modelling error is low. Moreover, the BL widths of the unmeasured states are compared to thresholds, if any BL width is above its threshold, the lower gain of the SVSF-L or Tanh-SVSF-L is used to correct the unmeasured state estimates. Otherwise, if all BL widths are below the thresholds, the EKF, UKF, or CKF gain is used to update the unmeasured state estimates.

1) EXTENDED KALMAN - LUENBERGER SMOOTH VARIABLE STRUCTURE FILTER (EK-SVSF-L)

Prediction: Given the a posteriori state estimate from the last time step, denoted as $\hat{\mathbf{x}}_{k|k}$, the predicted state is computed using the system model:

$$\hat{\mathbf{x}}_{k+1|k} = f(\hat{\mathbf{x}}_{k|k}, \mathbf{u}_k) \tag{3}$$

The covariance of the predicted state, also known as the a priori covariance (denoted as $\mathbf{P}_{k+1|k}$), is obtained via linearization similarly to the EKF [3]. It is assumed that the a posteriori state covariance is also given from the previous time step, denoted as $\mathbf{P}_{k|k}$. Similar to the EKF [3], linearization is applied to the estimated state trajectory by applying a Taylor series approximation to equation (1). This results in a Jacobian matrix \mathbf{F}_k , which is obtained as:

$$\mathbf{F}_k = \frac{\partial f(\hat{\mathbf{x}}_{k|k}, \mathbf{u}_k)}{\partial \mathbf{x}} \quad (4)$$

The Jacobian is then used to obtain the a priori error covariance matrix:

$$\mathbf{P}_{k+1|k} = \mathbf{F}_k \mathbf{P}_{k|k} \mathbf{F}_k^T + \mathbf{Q}_k = \begin{bmatrix} \mathbf{P}_{k+1|k}^{11} & \mathbf{P}_{k+1|k}^{12} \\ \mathbf{P}_{k+1|k}^{21} & \mathbf{P}_{k+1|k}^{22} \end{bmatrix} \quad (5)$$

Correction: The predicted measurement, innovation covariance, and a priori measurement error are obtained as:

$$\hat{\mathbf{z}}_{k+1|k} = \mathbf{H}_{k+1} \hat{\mathbf{x}}_{k+1|k} \quad (6)$$

$$\mathbf{S}_{k+1} = \mathbf{H}_{k+1} \mathbf{P}_{k+1|k} \mathbf{H}_{k+1}^T + \mathbf{R}_{k+1} \quad (7)$$

$$\mathbf{e}_{z,k+1|k} = \mathbf{z}_{k+1} - \hat{\mathbf{z}}_{k+1|k} \quad (8)$$

Since not all states are measured, the output matrix is non-square of dimensions $m \times n$, it follows the form defined in [22] and [34], which is expressed as:

$$\mathbf{H}_{k+1} = [\mathbf{H}_1 \ \mathbf{H}_2] \quad (9)$$

where \mathbf{H}_1 is $m \times m$ and \mathbf{H}_2 is a zero matrix of dimensions $m \times (n - m)$. m is the number of measured states and n is the number of states. Since a Luenberger observer is employed to estimate unmeasured states, using a similar procedure to [17] and [34], the state vector consists of two portions, the upper part represents the measured states, denoted by \mathbf{x}_{u_k} , and the lower portion contains the unmeasured states, \mathbf{x}_{l_k} , which is shown as follows:

$$\mathbf{x}_k = \begin{bmatrix} \mathbf{x}_{u_k} \\ \mathbf{x}_{l_k} \end{bmatrix} \quad (10)$$

The linearized system undergoes a transformation using a transformation matrix \mathbf{T} . Since the system model is non-linear, linearization is applied to that model before applying the transformation. The transformed transition matrix is:

$$\Phi_k = \mathbf{T} \mathbf{F}_k \mathbf{T}^{-1} = \begin{bmatrix} \Phi_{11} & \Phi_{12} \\ \Phi_{21} & \Phi_{22} \end{bmatrix} \quad (11)$$

When using a Luenberger observer to obtain unmeasured states, the error vectors associated with the measured and unmeasured states are denoted by \mathbf{E}_z and \mathbf{E}_y , respectively, which are [22]:

$$\mathbf{E}_z = |\mathbf{e}_{z,k+1|k}| + \gamma_z |\mathbf{e}_{z,k|k}| \quad (12)$$

$$\mathbf{E}_y = |\Phi_{22} \Phi_{12}^{-1} \mathbf{e}_{z,k+1|k}| + \gamma_y |\Phi_{12}^{-1} \mathbf{e}_{z,k+1|k}| \quad (13)$$

where the matrices γ_z and γ_y are diagonal matrices of dimensions $m \times m$ and $(n - m) \times (n - m)$, respectively, which are parameters. The diagonal elements can take values in the

ranges of $0 \leq \gamma_{z_{ii}} < 1$ and $0 \leq \gamma_{y_{ii}} < 1$. These parameters determine the filter's convergence rates [17], [34].

The next step is to obtain the Generalized Variable Boundary Layer (GVBL), which gives the boundary layer (BL) widths for the measured and unmeasured states. In [22], to obtain the GVBL, considering linear systems only, the trace of the a posteriori covariance matrix of the Luenberger SVSF from [34] was minimized with respect to the BL widths of the measured states and unmeasured states, represented as ψ_z and ψ_y , respectively. For linear systems, the smoothing BL widths were found to be [22]:

$$\psi_z = (\bar{\mathbf{E}}_z^{-1} \mathbf{H}_1 \mathbf{P}_{k+1|k}^{11} \mathbf{H}_1^T \mathbf{S}_{k+1}^{-1})^{-1} \quad (14)$$

$$\psi_y = (\bar{\mathbf{E}}_y^{-1} \mathbf{P}_{k+1|k}^{21} \mathbf{H}_1^T \mathbf{S}_{k+1}^{-1} (\Phi_{22} \Phi_{12}^{-1})^{-1})^{-1} \quad (15)$$

where $\bar{\mathbf{E}}_z = \text{diag}(\mathbf{E}_z)$ and $\bar{\mathbf{E}}_y = \text{diag}(\mathbf{E}_y)$. Note that even though the BL widths above are for linear systems, they can be applied to nonlinear systems by using Φ_{12} and Φ_{22} from the transformed linearized state transition matrix from equation (11). These BL widths are used as a means to combine SVSF-L with EKF by comparing these widths to thresholds as discussed later below.

Next, the EKF gain is computed [3]:

$$\mathbf{K}_{k+1}^{EKF} = \mathbf{P}_{k+1|k} \mathbf{H}_{k+1}^T \mathbf{S}_{k+1}^{-1} = \begin{bmatrix} \mathbf{K}_{k+1}^{EKF} \\ \mathbf{K}_{k+1}^{EKF} \end{bmatrix} \quad (16)$$

where $\mathbf{K}_{u_{k+1}}^{EKF}$ is an $m \times m$ gain matrix for the measured states and $\mathbf{K}_{l_{k+1}}^{EKF}$ is an $(n - m) \times m$ matrix for the unmeasured states.

After, the task is to select the upper and lower gains, which are also known as the observed and unobserved gains, respectively. The observed gain updates the measured states, and the unobserved gain corrects the unmeasured states. The stacked gain is denoted by:

$$\mathbf{K}_{k+1} = \begin{bmatrix} \mathbf{K}_{u_{k+1}} \\ \mathbf{K}_{l_{k+1}} \end{bmatrix} \quad (17)$$

Let $\psi_{z,max}$ and $\psi_{y,max}$ be vectors containing the upper limits/thresholds for the level of modelling uncertainty for the measured and unmeasured states, respectively. The smoothing boundary layer widths measure the level of modelling error for each state as described in [22] and [29]. Hence, they are compared to their upper limits as described below to determine whether to apply the SVSF-L gains or EKF gains. When the widths are low, this indicates the level of modelling error is low, which makes a nonlinear KF advantageous. When the widths are high, the modelling uncertainty is high, thus, the SVSF-L is more beneficial in order to maintain robustness and stability against modelling uncertainties. Note that the SVSF-L gains below are from [22] and [34]:

If the BL widths for each state in ψ_z are below their respective limits in $\psi_{z,max}$, then

$$\mathbf{K}_{u_{k+1}} = \mathbf{K}_{u_{k+1}}^{EKF} \quad (18)$$

else:

$$\mathbf{K}_{u_{k+1}} = \mathbf{K}_{u_{k+1}}^{SVSFL}$$

$$= \mathbf{H}_1^{-1} \text{diag}[\mathbf{E}_z \circ \text{sat}(\mathbf{e}_{z,k+1|k}, \boldsymbol{\psi}_{z,max})][\text{diag}(\mathbf{e}_{z,k+1|k})]^{-1} \quad (19)$$

If the BL widths for each state in $\boldsymbol{\psi}_y$ are below their respective limits in $\boldsymbol{\psi}_{y,max}$, then

$$\mathbf{K}_{l_{k+1}} = \mathbf{K}_{l_{k+1}}^{EKF} \quad (20)$$

else:

$$\begin{aligned} \mathbf{K}_{l_{k+1}} &= \mathbf{K}_{l_{k+1}}^{SVSF} \\ &= \text{diag}[\mathbf{E}_y \circ \text{sat}(\Phi_{22} \Phi_{12}^{-1} \mathbf{e}_{z,k+1|k}, \boldsymbol{\psi}_{y,max})] \\ &\quad [\text{diag}(\Phi_{22} \Phi_{12}^{-1} \mathbf{e}_{z,k+1|k})]^{-1} \Phi_{22} \Phi_{12}^{-1} \end{aligned} \quad (21)$$

where \circ refers to the Schur product. The saturation function denoted by $\text{sat}()$ is used to smoothen the discontinuous corrective action from the switching gain. In terms of how the function works, as explained in [17], let \mathbf{q} and $\boldsymbol{\psi}$ be vectors of the same dimension, $\text{sat}(\mathbf{q}, \boldsymbol{\psi})$ outputs a vector of the same dimension, where the i th component of the vector is computed as:

$$\text{sat}_i(\mathbf{q}, \boldsymbol{\psi}) = \begin{cases} \frac{q_i}{\psi_i}, & \text{if } |\frac{q_i}{\psi_i}| \leq 1 \\ \text{sign}(\frac{q_i}{\psi_i}), & \text{if } |\frac{q_i}{\psi_i}| > 1 \end{cases} \quad (22)$$

The a posteriori state estimate, covariance, and measurement error are computed as:

$$\hat{\mathbf{x}}_{k+1|k+1} = \begin{bmatrix} \hat{\mathbf{x}}_{u_{k+1|k}} \\ \hat{\mathbf{x}}_{l_{k+1|k}} \end{bmatrix} + \begin{bmatrix} \mathbf{K}_{u_{k+1}} \\ \mathbf{K}_{l_{k+1}} \end{bmatrix} \mathbf{e}_{z,k+1|k} \quad (23)$$

$$\begin{aligned} \mathbf{P}_{k+1|k+1} &= \mathbf{P}_{k+1|k} - \begin{bmatrix} \mathbf{K}_{u_{k+1}} \\ \mathbf{K}_{l_{k+1}} \end{bmatrix} \mathbf{H}_{k+1} \mathbf{P}_{k+1|k} \\ &\quad - \mathbf{P}_{k+1|k} \mathbf{H}_{k+1}^T \begin{bmatrix} \mathbf{K}_{u_{k+1}} \\ \mathbf{K}_{l_{k+1}} \end{bmatrix}^T \\ &\quad + \begin{bmatrix} \mathbf{K}_{u_{k+1}} \\ \mathbf{K}_{l_{k+1}} \end{bmatrix} \mathbf{S}_{k+1} \begin{bmatrix} \mathbf{K}_{u_{k+1}} \\ \mathbf{K}_{l_{k+1}} \end{bmatrix}^T \end{aligned} \quad (24)$$

$$\mathbf{e}_{z,k+1|k+1} = \mathbf{z}_{k+1} - \mathbf{H}_{k+1} \hat{\mathbf{x}}_{k+1|k+1} \quad (25)$$

2) UNSCENTED KALMAN - LUENBERGER SMOOTH VARIABLE STRUCTURE FILTER (UK-SVSF-L)

Many of the equations for this filter are the same as the EK-SVSF-L, the only differences are that the predicted state, a priori covariance, predicted measurement, and innovation covariance are computed differently. Thus, equations (3), (5), (6), and (7) are replaced by the formulas of $\hat{\mathbf{x}}_{k+1|k}$, $\mathbf{P}_{k+1|k}$, $\hat{\mathbf{z}}_{k+1|k}$, and \mathbf{S}_{k+1} shown below, respectively. Also, the EKF gain is replaced with the UKF gain, hence, the EKF gains from equations (18) and (20) are replaced by the observed and unobserved gains of the UKF, respectively. The predicted state, a priori covariance, predicted measurement, innovation covariance, and UKF gain are calculated as follows:

In the prediction stage, sigma points are used to compute the predicted state and covariance as described in [7]. The $2n+1$ sigma points and their corresponding weighting factors are obtained as:

$$\boldsymbol{\chi}_{0,k|k} = \hat{\mathbf{x}}_k \quad i = 0 \quad (26)$$

$$\boldsymbol{\chi}_{i,k|k} = \hat{\mathbf{x}}_{k|k} + (\sqrt{(n+\lambda)\mathbf{P}_{k|k}})_i \quad i = 1 \dots n \quad (27)$$

$$\boldsymbol{\chi}_{i,k|k} = \hat{\mathbf{x}}_{k|k} - (\sqrt{(n+\lambda)\mathbf{P}_{k|k}})_i \quad i = n+1 \dots 2n \quad (28)$$

$$W_0^x = \frac{\lambda}{n+\lambda} \quad (29)$$

$$W_0^p = \frac{\lambda}{n+\lambda} + (1 - \alpha^2 + \beta) \quad (30)$$

$$W_i = \frac{1}{2(n+\lambda)} \quad i = 1 \dots 2n \quad (31)$$

where λ is a scaling parameter as described in [7], which is calculated as $\lambda = \alpha^2(n + \kappa) - n$ and n is the number of states [5]. κ is also a scaling parameter. The term α represents the spread of sigma points around the mean of the state vector and β is a parameter used to take into account a-priori knowledge of the state vector's probability distribution [7]. $(\sqrt{(n+\lambda)\mathbf{P}_{k|k}})_i$ is the i th column of the square root of the $(n+\lambda)\mathbf{P}_{k|k}$ matrix. Next, the points are propagated through the non-linear state transition function to get the predicted state and covariance:

$$\boldsymbol{\chi}_{i,k+1|k} = \mathbf{f}(\boldsymbol{\chi}_{i,k|k}, \mathbf{u}_k) \quad (32)$$

$$\hat{\mathbf{x}}_{k+1|k} = \sum_{i=0}^{2n} W_i \boldsymbol{\chi}_{i,k+1|k} \quad (33)$$

$$\begin{aligned} \mathbf{P}_{k+1|k} &= \sum_{i=0}^{2n} W_i (\boldsymbol{\chi}_{i,k+1|k} - \hat{\mathbf{x}}_{k+1|k})(\boldsymbol{\chi}_{i,k+1|k} - \hat{\mathbf{x}}_{k+1|k})^T \\ &\quad + \mathbf{Q} \\ &= \begin{bmatrix} \mathbf{P}_{k+1|k}^{11} & \mathbf{P}_{k+1|k}^{12} \\ \mathbf{P}_{k+1|k}^{21} & \mathbf{P}_{k+1|k}^{22} \end{bmatrix} \end{aligned} \quad (34)$$

The predicted measurement and innovation covariance are calculated also using sigma points using the method explained in [7]:

$$\mathbf{Z}_{i,k+1|k} = \mathbf{h}(\boldsymbol{\chi}_{i,k+1|k}, \mathbf{u}_k) \quad (35)$$

$$\hat{\mathbf{z}}_{k+1|k} = \sum_{i=0}^{2n} W_i \mathbf{Z}_{i,k+1|k} \quad (36)$$

$$\begin{aligned} \mathbf{S}_{k+1} &= \sum_{i=0}^{2n} W_i (\mathbf{Z}_{i,k+1|k} - \hat{\mathbf{z}}_{k+1|k})(\mathbf{Z}_{i,k+1|k} - \hat{\mathbf{z}}_{k+1|k})^T \\ &\quad + \mathbf{R}_{k+1} \end{aligned} \quad (37)$$

The cross covariance is [7]:

$$\mathbf{P}_{xz,k+1|k} = \sum_{i=0}^{2n} W_i (\boldsymbol{\chi}_{i,k+1|k} - \hat{\mathbf{x}}_{k+1|k})(\mathbf{Z}_{i,k+1|k} - \hat{\mathbf{z}}_{k+1|k})^T \quad (38)$$

The UKF gain is computed as [7]:

$$\mathbf{K}_{k+1}^{UKF} = \mathbf{P}_{xz,k+1|k} \mathbf{S}_{k+1}^{-1} = \begin{bmatrix} \mathbf{K}_{k+1}^{UKF} \\ \mathbf{K}_{k+1}^{UKF} \end{bmatrix} \quad (39)$$

where \mathbf{K}_{k+1}^{UKF} is an $m \times m$ observed gain matrix for the measured states and \mathbf{K}_{k+1}^{UKF} is an $(n-m) \times m$ gain matrix for the unmeasured states.

3) CUBATURE KALMAN - LUENBERGER SMOOTH VARIABLE STRUCTURE FILTER (CK-SVSF-L)

Most equations of this filter are the same as EK-SVSF-L. The only differences are that the predicted state, a priori covariance, predicted measurement, and innovation covariance are computed differently. Hence, equations (3), (5), (6), and (7) are replaced by the computations of $\hat{\mathbf{x}}_{k+1|k}$, $\mathbf{P}_{k+1|k}$, $\hat{\mathbf{z}}_{k+1|k}$, and \mathbf{S}_{k+1} shown below, respectively. In addition, the EKF gain is replaced with the CKF gain. The calculations of these quantities are as follows:

Cubature points are used to obtain the predicted state and a priori covariance using the method described in [39]. The $2n$ Cubature points are obtained as:

$$\mathbf{x}_{i,k|k} = \hat{\mathbf{x}}_{k|k} + \sqrt{n}(\sqrt{\mathbf{P}_{k|k}})_i \quad i = 1 \dots n \quad (40)$$

$$\mathbf{x}_{i,k|k} = \hat{\mathbf{x}}_{k|k} - \sqrt{n}(\sqrt{\mathbf{P}_{k|k}})_i \quad i = n + 1 \dots 2n \quad (41)$$

where n is the number of states. $(\sqrt{\mathbf{P}_{k|k}})_i$ is the i th column of the square root of the $\mathbf{P}_{k|k}$ matrix.

The predicted state and its associated covariance are calculated as [39]:

$$\mathbf{x}_{i,k+1|k} = f(\mathbf{x}_{i,k|k}, \mathbf{u}_k) \quad (42)$$

$$\hat{\mathbf{x}}_{k+1|k} = \frac{1}{2n} \sum_{i=1}^{2n} \mathbf{x}_{i,k+1|k} \quad (43)$$

$$\begin{aligned} \mathbf{P}_{k+1|k} &= \frac{1}{2n} \sum_{i=1}^{2n} (\mathbf{x}_{i,k+1|k} - \hat{\mathbf{x}}_{k+1|k})(\mathbf{x}_{i,k+1|k} - \hat{\mathbf{x}}_{k+1|k})^T \\ &+ \mathbf{Q}_k \end{aligned} \quad (44)$$

The predicted measurement and innovation covariance are calculated using Cubature points as described in [39]:

$$\mathbf{Z}_{i,k+1|k} = h(\mathbf{x}_{i,k+1|k}, \mathbf{u}_k) \quad (45)$$

$$\hat{\mathbf{z}}_{k+1|k} = \frac{1}{2n} \sum_{i=1}^{2n} \mathbf{Z}_{i,k+1|k} \quad (46)$$

$$\begin{aligned} \mathbf{S}_{k+1} &= \frac{1}{2n} \sum_{i=1}^{2n} (\mathbf{Z}_{i,k+1|k} - \hat{\mathbf{z}}_{k+1|k})(\mathbf{Z}_{i,k+1|k} - \hat{\mathbf{z}}_{k+1|k})^T \\ &+ \mathbf{R}_{k+1} \end{aligned} \quad (47)$$

The cross covariance is [39]:

$$\mathbf{P}_{\mathbf{xz},k+1|k} = \frac{1}{2n} \sum_{i=1}^{2n} (\mathbf{x}_{i,k+1|k} - \hat{\mathbf{x}}_{k+1|k})(\mathbf{Z}_{i,k+1|k} - \hat{\mathbf{z}}_{k+1|k})^T \quad (48)$$

The CKF gain is computed as [39]:

$$\mathbf{K}_{k+1}^{CKF} = \mathbf{P}_{\mathbf{xz},k+1|k} \mathbf{S}_{k+1}^{-1} = \begin{bmatrix} \mathbf{K}_{k+1}^{CKF} \\ \mathbf{K}_{k+1}^{CKF} \end{bmatrix} \quad (49)$$

where \mathbf{K}_{k+1}^{CKF} is an $m \times m$ gain matrix for the measured states and \mathbf{K}_{k+1}^{CKF} is an $(n - m) \times m$ gain matrix for the unmeasured states.

4) EXTENDED KALMAN - LUENBERGER HYPERBOLIC TANGENT SVSF (EK-TANH-SVSF-L)

The majority of the equations of this method are the same as EK-SVSF-L. Only the BL widths for the measured and unmeasured states as well as the SVSF gains are computed differently. Equations (14), (15), (19), and (21) are replaced by the calculations of ψ_z , ψ_y , $\mathbf{K}_{u_{k+1}}^{Tanh-SVSF}$, and $\mathbf{K}_{l_{k+1}}^{Tanh-SVSF}$, respectively, as shown below. These quantities are calculated as follows:

The Nonlinear Variable Boundary Layer (NVBL) reported in [38] is used to obtain the smoothing boundary layer (BL) widths for the measured and unmeasured states. In [38], the NVBL was obtained by minimizing the trace of the a posteriori covariance matrix of the Tanh-SVSF-L considering linear systems only. The minimization was done with respect to the BL widths of the measured states and unmeasured states, represented as ψ_z and ψ_y , respectively. The BL widths obtained from the NVBL are [38]:

$$\begin{aligned} \psi_z &= [\text{artanh}(\mathbf{H}_1 \mathbf{P}_{k+1|k}^{11} \mathbf{H}_1^T \mathbf{S}_{k+1}^{-1} \text{diag}(\mathbf{e}_{z,k+1|k}) \bar{\mathbf{E}}_z^{-1}) \\ &[\text{diag}(\mathbf{e}_{z,k+1|k})]^{-1}]^{-1} \end{aligned} \quad (50)$$

$$\begin{aligned} \psi_y &= [\text{artanh}(\mathbf{P}_{k+1|k}^{21} \mathbf{H}_1^T \mathbf{S}_{k+1}^{-1} \Phi_{12} \Phi_{22}^{-1} \\ &\text{diag}(\Phi_{22} \Phi_{12}^{-1} \mathbf{e}_{z,k+1|k}) \bar{\mathbf{E}}_y^{-1}) [\text{diag}(\Phi_{22} \Phi_{12}^{-1} \mathbf{e}_{z,k+1|k})]^{-1}]^{-1} \end{aligned} \quad (51)$$

where $\text{artanh}(\mathbf{A})$ applies the scalar inverse hyperbolic tangent function to every element in the matrix \mathbf{A} , assuming \mathbf{A} is a square matrix. Even though ψ_z and ψ_y are for linear systems, these widths can again be used for nonlinear systems by using Φ_{22} and Φ_{12} from the transformed linearized state transition matrix Φ .

The observed and unobserved gains are now [37]:

$$\begin{aligned} \mathbf{K}_{u_{k+1}}^{Tanh-SVSF} &= \mathbf{H}_1^{-1} \text{diag}[\mathbf{E}_z \circ \text{Tanh}(\mathbf{e}_{z,k+1|k}, \psi_{z,max})] \\ &[\text{diag}(\mathbf{e}_{z,k+1|k})]^{-1} \end{aligned} \quad (52)$$

$$\begin{aligned} \mathbf{K}_{l_{k+1}}^{Tanh-SVSF} &= \text{diag}[\mathbf{E}_y \circ \text{Tanh}(\Phi_{22} \Phi_{12}^{-1} \mathbf{e}_{z,k+1|k}, \psi_{y,max})] \\ &[\text{diag}(\Phi_{22} \Phi_{12}^{-1} \mathbf{e}_{z,k+1|k})]^{-1} \Phi_{22} \Phi_{12}^{-1} \end{aligned} \quad (53)$$

The $\text{Tanh}()$ function is used to smoothen the chattering resulting from the SVSF gain. The above Tanh-SVSF gains are from [37], which are modified SVSF gains. In [37], the $\text{sat}()$ function of the standard SVSF is replaced with $\text{Tanh}()$ to smoothen the chattering signal more effectively. Given that \mathbf{q} and ψ are vectors of the same dimensions, $\text{Tanh}(\mathbf{q}, \psi)$ outputs a vector of the same dimension, where the i th element of $\text{Tanh}(\mathbf{q}, \psi)$ is computed as:

$$\text{Tanh}(q_i, \psi_i)_i = \frac{e^{\frac{2q_i}{\psi_i}} - 1}{e^{\frac{2q_i}{\psi_i}} + 1} \quad (54)$$

5) UNSCENTED KALMAN - LUENBERGER HYPERBOLIC TANGENT SMOOTH VARIABLE STRUCTURE FILTER (UK-TANH-SVSF-L)

Most equations of this method are the same as UK-SVSF-L. Only ψ_z , ψ_y , the observed SVSF gain, and the unobserved

SVSF gain are computed differently. The equations for these variables are given in the previous sub-section.

6) CUBATURE KALMAN - LUENBERGER HYPERBOLIC TANGENT- SMOOTH VARIABLE STRUCTURE FILTER (CK-TANH-SVSF-L)

Similarly, the majority of the equations of this filter are the same as CK-SVSF-L. Only ψ_z, ψ_y , the observed SVSF gain, and the unobserved SVSF gain are computed differently. The equations for these quantities are given in the sub-section that presents EK-Tanh-SVSF-L.

III. SIMULATION RESULTS

To evaluate the performance of the proposed framework, a scenario of a maneuvering aircraft is simulated that undergoes turns, and the objective is to apply filters to track the aircraft using noisy position-only measurements from a radar. The six filters resulting from the proposed framework are compared to the EKF, UKF, CKF, PF, three SVSF variants that deploy EKF UKF, and CKF presented in [30] and [31], and two SVSF variants in [40], which deploy linearization and sigma points. The following nonlinear motion model is used to generate the aircraft trajectory:

$$\mathbf{x}_{k+1} = \mathbf{f}(\mathbf{x}_k) + \mathbf{v}_k \tag{55}$$

$$\mathbf{v}_k \sim N(\mathbf{0}, \mathbf{Q}_k) \tag{56}$$

The state variables are x -position, y -position, x -velocity, y -velocity, and turn-rate, represented as $p_{xk}, p_{yk}, v_{xk}, v_{yk}$, and ω_k , respectively. In the equations below, T_s represents the sampling time.

Considering the nonlinear Coordinated Turn (CT) model [4], the model's state equation is obtained as follows:

$$\mathbf{x}_k = [p_{xk} \ p_{yk} \ v_{xk} \ v_{yk} \ \omega_k]^T \tag{57}$$

$$\mathbf{f}(\mathbf{x}_k) = \begin{bmatrix} p_{xk} + \frac{\sin(\omega_k T_s)}{w_k} v_{xk} - \frac{1 - \cos(\omega_k T_s)}{w_k} v_{yk} \\ p_{yk} + \frac{1 - \cos(\omega_k T_s)}{w_k} v_{xk} + \frac{\sin(\omega_k T_s)}{w_k} v_{yk} \\ \cos(\omega_k T_s) v_{xk} - \sin(\omega_k T_s) v_{yk} \\ \sin(\omega_k T_s) v_{xk} + \cos(\omega_k T_s) v_{yk} \\ \omega_k \end{bmatrix} \tag{58}$$

$$\mathbf{Q}_k = L_1 \begin{bmatrix} \frac{T_s^3}{3} & 0 & \frac{T_s^2}{2} & 0 & 0 \\ 0 & \frac{T_s^3}{3} & 0 & \frac{T_s^2}{2} & 0 \\ \frac{T_s^2}{2} & 0 & T_s & 0 & 0 \\ 0 & \frac{T_s^2}{2} & 0 & T_s & 0 \\ 0 & 0 & 0 & 0 & \frac{L_2 T_s}{L_1} \end{bmatrix} \tag{59}$$

The terms L_1 and L_2 are power spectral densities [4].

It is assumed that a radar obtains the position of the aircraft, hence, the measurement model is defined as:

$$\mathbf{z}_k = \mathbf{H}_k \mathbf{x}_k + \mathbf{w}_k \tag{60}$$

$$\mathbf{w}_k \sim N(\mathbf{0}, \mathbf{R}_k) \tag{61}$$

$$\mathbf{H}_k = \begin{bmatrix} 1 & 0 & 0 & 0 & 0 \\ 0 & 1 & 0 & 0 & 0 \end{bmatrix} \tag{62}$$

In the considered scenario, similar to [39], an aircraft maneuvers and its trajectory is generated using the CT model. To highlight the advantage of the proposed framework in handling model mismatch, two consecutive turns were included in the target trajectory as shown in Figure 3. Since the CT model represents a single turn, a sequence of turns cannot be captured by this model, hence, such a sequence leads to model mismatch. In the first 49 s of the simulation, the aircraft turns with a turn-rate of 3°/s and afterwards, it turns in the opposite direction at -3°/s. Therefore, the model mismatch occurs in the trajectory at 50 s on-wards. In terms of the parameters used to generate the trajectory, the sampling time T_s was set to 1 s and the power spectral densities used in the process noise covariance were set to $L_1 = 0.001$ and $L_2 = 1.75 \times 10^{-5}$. It was assumed that only the position of the aircraft was measured. The measurements were generated with a noise standard deviation of 50 m. The initial x and y positions of the aircraft were 1000 m and 1000 m, respectively. The initial velocity in the x direction was 300 m/s and the initial turn-rate was 3°/s. For performance evaluation, the synthetically generated trajectory of Figure 3 was used as the ground truth to compute the root mean square error (RMSE) as a measure of estimation accuracy.

A. PERFORMANCE METRICS

Three types of performance metrics are utilized, one computes the overall scalar state estimation RMSE of a specific state variable, another computes RMSE across multiple state variables, and the other computes the position and velocity RMSE overtime.

Let x_j be the j th state variable from the state vector \mathbf{x}_k . The scalar RMSE of a specific state variable x_j is computed as:

$$\text{RMSE}_{x_j} = \sqrt{\frac{1}{M * N} \sum_{i=1}^M \sum_{k=0}^N (\hat{x}_{j|k}^i - x_{jk})^2} \tag{63}$$

where M is the total number of Monte Carlo runs, N is the total number of time steps in one Monte Carlo run including the time step of the initial state, x_{jk} represents the true value of the state x_j at time step k , and $\hat{x}_{j|k}^i$ represents the estimate of x_j at time step k from Monte Carlo run i . A normalized RMSE (NRMSE) is also calculated to compute the RMSE over multiple state variables. Each state variable's RMSE is normalized by the range of the state variable because not all states have the same range of values and units, and the range is defined by $|x_j^{max} - x_j^{min}|$. The NRMSE is calculated as:

$$\text{NRMSE} = \sum_{j=1}^n \frac{\text{RMSE}_{x_j}}{|x_j^{max} - x_j^{min}|} \tag{64}$$

where n is the number of states, x_j^{max} is the maximum value of x_j , and x_j^{min} is the minimum value of x_j .

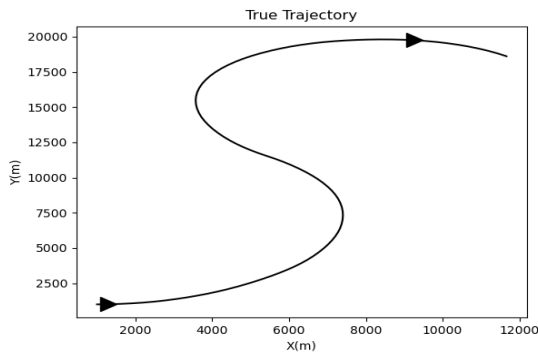


FIGURE 3. True aircraft trajectory.

The position and velocity RMSE at time step k is calculated as follows:

$$\text{RMSE}_{p_k} = \sqrt{\frac{1}{M} \sum_{i=1}^M [(\hat{p}_{x_k|k}^i - p_{x_k})^2 + (\hat{p}_{y_k|k}^i - p_{y_k})^2]} \quad (65)$$

$$\text{RMSE}_{v_k} = \sqrt{\frac{1}{M} \sum_{i=1}^M [(\hat{v}_{x_k|k}^i - v_{x_k})^2 + (\hat{v}_{y_k|k}^i - v_{y_k})^2]} \quad (66)$$

The terms p_{x_k} , p_{y_k} , v_{x_k} , and v_{y_k} represent the true x position, y position, x velocity, and y velocity at time step k , respectively, whereas, the terms $\hat{p}_{x_k|k}^i$, $\hat{p}_{y_k|k}^i$, $\hat{v}_{x_k|k}^i$, and $\hat{v}_{y_k|k}^i$, represent the estimated x position, y position, x velocity, and y velocity, at time step k from Monte Carlo run i , respectively.

B. SETTINGS AND PARAMETERS

To make a fair comparison, all filters were run using the CT model with the same model parameters and the same initial conditions. The filter parameters are listed in Table 2. 1-point initialization [4] was applied to initialize the state and covariance of each filter. Using this initialization technique [4], the initial state and covariance were set to $\hat{\mathbf{x}}_{0|0} = [z_{x_0} \ z_{y_0} \ 0 \ 0 \ 0]^T$ and $\mathbf{P}_{0|0} = \text{diag}([\sigma_x^2 \ \sigma_y^2 \ v_{max}^2 \ v_{max}^2 \ \omega_{max}^2])$, respectively. Where z_{x_0} and z_{y_0} are the initial x and y position measurements received by the radar, respectively. σ_x and σ_y represent the measurement noise standard deviation in each coordinate, both are 50 m. v_{max} and ω_{max} are the maximum velocity and turn-rate, which were set to 300 m/s and 3°/s, respectively. The parameters of all filters were tuned such that they provide optimal performance under the presence of no model mismatch, thus, the parameters were chosen to minimize the RMSE of each state for the first 49 s of the simulation because there is no modelling error before 50 s. It was assumed that the modelling error that occurs at 50 s on-wards is not prior knowledge. For tuning the nonlinear KFs, it is conceptually clear that the \mathbf{Q}_k and \mathbf{R}_k used to generate the true trajectory and synthetic measurements are optimal for the first 49 s. Hence, the process noise covariance \mathbf{Q}_k in (59) was set with the same values for L_1 and L_2 , which were used to obtain the ground truth. The measurement noise covariance and sampling time T_s were

set as $\mathbf{R}_k = \text{diag}([50^2, 50^2])$ and 1 s, respectively. For the UKF parameters α , β , and κ , to see if other values provide better performance compared to the default ones, a Genetic Algorithm (GA) known as Non-dominated Sorting Genetic Algorithm (NSGA-II) [41] was used to search for parameter values that minimize the RMSE of each state variable for the first 49 s of the simulation. This algorithm is used to solve multi-objective optimization problems, where the goal is to minimize multiple objective functions. Each objective function in this case is the scalar RMSE of a state variable. In this case, each scalar RMSE is calculated using equation (63), but the only differences are that the number of samples N and the number of runs M take different values. N is set to the point that corresponds to 49 s since the goal is to minimize RMSE in the presence of no modelling error and M is set to 5. Since there are 5 state variables, there are 5 objective functions. It was found that no significant performance improvement is achieved using the optimal parameter values obtained by NSGA-II to track the target for the first 49 s compared to using the default values. The RMSE of the state estimates were quite comparable to those of default values with very marginal differences. Thus, α , β , and κ were set to default values of 0.001, 2, and 0, respectively. A value of 2 for β is optimal for Gaussian distributions as stated in [7]. The measurement and system noise is Gaussian for the first 49 s of the simulation, hence, $\beta = 2$ is optimal. The UK-SVSF-L and UK-Tanh-SVSF-L use the same values for α , β , and κ .

Parameters of the PF were also tuned such that the performance is optimal when there is no modelling error, thus, NSGA-II was used to minimize the RMSE of each state for the first 49 s of the simulation. The optimal number of particles and the minimum effective particle ratio were found to be 1408603 and 0.8895, respectively. The multi-nominal sampling strategy was chosen.

The three filters presented in [30] and [31] require a full measurement matrix, hence, \mathbf{R}_k is 5×5 for these filters. For the filters presented in [31], the authors used available measurements to derive artificial measurements of unmeasured states to make $\mathbf{H}_k = \mathbf{I}$. Artificial velocity measurements were obtained via numerical differentiation as follows:

$$z_k^{v_x} = \frac{z_k^x - z_{k-1}^x}{T_s} \quad (67)$$

$$z_k^{v_y} = \frac{z_k^y - z_{k-1}^y}{T_s} \quad (68)$$

Note that backward differencing is done instead of forward differencing in [31], since it is not practical to assume the future measurement is available. z_k^x and z_k^y are the x and y position measurements obtained from the radar at time step k , respectively. These are obtained from equation (60). $z_k^{v_x}$ and $z_k^{v_y}$ are the artificial x and y velocities, respectively. The artificial turn-rate measurement was set to zero, with $z_k^\omega = 0^\circ/\text{s}$, as it is impossible to derive an artificial measurement for it given position-only measurements.

TABLE 2. Filter Parameters.

Parameter	Values
$\hat{\mathbf{x}}_{0 0}$	$[z_{x0} \ z_{y0} \ 0 \ 0 \ 0]^T$
$\mathbf{P}_{0 0}$	$\text{diag}([\sigma_x^2 \ \sigma_y^2 \ v_{max}^2 \ v_{max}^2 \ \omega_{max}^2])$
T_s	1s
\mathbf{Q}_k	Equation (59) with $L_1 = 0.001$ and $L_2 = 1.75 \times 10^{-5}$
\mathbf{R}_k	$\text{diag}([50^2, 50^2])$
\mathbf{R}_k for [30], [31]	$\text{diag}([50^2, 50^2, 5000, 5000, (10^{-5})^2])$
α	0.001
β	2
κ	0
Number of Particles	1408603
Minimum Effective Particle Ratio	0.8895
ψ_{max}	$[260.902 \ 260.902 \ 376.975 \ 376.975 \ 110.54]^T$
$\psi_{z,max}$	$[260.902 \ 260.902]^T$
$\psi_{y,max}$	$[3559.88 \ 3559.88 \ 110.54]^T$
γ	0.1I
γ_z	0.1I
γ_y	0.1I
\mathbf{T}	I

To obtain \mathbf{R}_k , variances of the artificial measurements are necessary, for z_k^x and z_k^y , they are equal to $\frac{2\sigma_x^2}{T_s^2}$ and $\frac{2\sigma_y^2}{T_s^2}$, respectively. Substituting the assumed values for σ_x , σ_y , and T_s in these two relations results in 5000 for both. The variance of the artificial turn-rate of 0°/s is set to $(10^{-5})^2$ instead of zero to maintain numerical stability in the filters. Therefore, $\mathbf{R}_k = \text{diag}([50^2, 50^2, 5000, 5000, (10^{-5})^2])$ for the filters of [30] and [31].

The boundary layer (BL) parameters were obtained through minimizing the RMSE of each state variable for the first 49 s using the NSGA-II to obtain optimal parameters under the presence of no model mismatch. In terms of the BL parameters, the proposed filters use values of $\psi_{z,max} = [260.902 \ 260.902]^T$ and $\psi_{y,max} = [3559.88 \ 3559.88 \ 110.54]^T$, where the elements in $\psi_{z,max}$ contain the upper limits on the BL widths for the x and y position. The elements in $\psi_{y,max}$ contain the upper limits for the BL widths of the x and y velocity as well as the turn-rate. For the three filters presented in [30] and [31], the BL parameter was set to $\psi_{max} = [260.902 \ 260.902 \ 376.975 \ 376.975 \ 110.54]^T$, which contains the upper limits on the BL widths for x and y position, x and y velocity, and turn-rate. The reason that the upper limit for the velocities were chosen to be lower for these three filters (EK-SVSF-I, UK-SVSF-I, CK-SVSF) compared to the proposed methods is that there is an artificial measurement associated with the velocities in the former, whereas for the proposed approaches, the upper limits are much higher because the proposed filters did not take velocity measurements. These are higher because the existence subspace is large for states with no associated measurements according to [42] when applying a reduced-order observer to estimate unmeasured states. All proposed filters use a reduced-order observer to estimate unmeasured states. Lastly, for the two filters presented in [40], the BL widths must

be specified only for measured states, hence, the parameter was set as $\psi_z = [260.902 \ 260.902]^T$. The convergence rate parameters in all SVSF filters was set to 0.1I, which are denoted by γ , γ_z , and γ_y in Table 2. The filters of [31] and [30] use γ , and the proposed filters use γ_z and γ_y . The strategies of [40] use γ_z only. The transformation matrix \mathbf{T} used in the proposed filters was set to I. The number of Monte Carlo runs was 1000.

C. RESULTS

Table 3 shows the estimation RMSE for each state, equation (63) was used to obtain the scalar RMSE of each state. The table also includes the NRMSE of each filter. According to the last six rows of the table, the proposed methods perform the best for state estimation overall in terms of NRMSE, which is explained in this sub-section. They provide superior performance for estimating position and velocity based on the scalar RMSE estimates of these states. Figures 4 and 5 show the position and velocity RMSE over-time for each state estimator, equations (65) and (66) were utilized to obtain these graphs. Prior to 50 s, which is before the aircraft turns in the opposite direction, the EKF, UKF, CKF, and PF have the best performance as shown in Figures 4b and 5b. This is because there is not much modelling uncertainty before 50 s since the filter model is accurate. Thus, these filters are expected to perform better when there is no model mismatch.

Once the target turns in the opposite direction, the performance of the EKF, UKF, CKF, and PF starts to degrade in Figures 4c, 4e, 5c, and 5e because the model they use is not valid anymore, and this has a negative impact on robustness and stability since these filters assume a precisely known model. Since the CT model is used for only one turn and it assumes the turn-rate to be nearly constant, it cannot model multiple turns. Thus, filter model mismatch is present at 50 s and beyond from the negated turn-rate. Figures 4c and 5c show the position and velocity RMSE around the time the

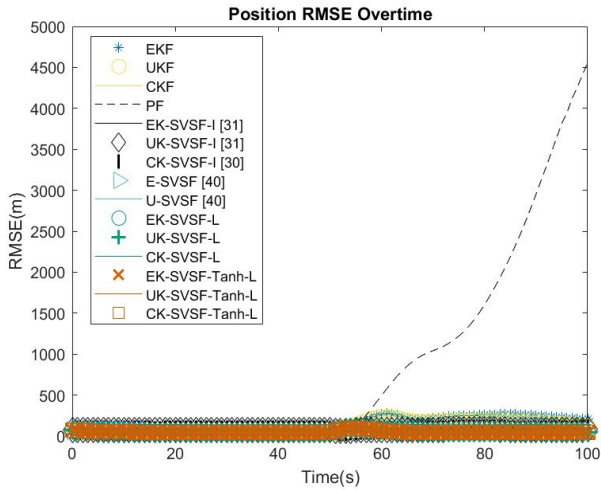
target turns in the opposite direction. It can be observed that in both figures, as soon as the aircraft turns in the opposite direction, the RMSE starts to increase at 50 s, which is due to modelling error. In Figures 4a, 4e, 5a, and 5e the PF becomes unstable because of model mismatch, resulting in the highest NRMSE in Table 3. The PF also requires a strictly known model likewise to the EKF, UKF, and CKF. All SVSF variants perform better compared to the EKF, UKF, CKF, and PF at 50 s on-wards for position estimation as shown in Figures 4c and 4e as well as Table 3. This can be attributed to their stability and robustness against modelling errors due to using the switching gain. As illustrated in Figures 4d and 4e, the gain causes the estimated position to converge closer to the ground truth. In Figures 4b and 4d, in the zoomed in parts, the RMSE of the filters using Tanh-SVSF-L is in general slightly lower than the filters using SVSF-L due to greater chattering attenuation from the Tanh-SVSF gain. In [37], it is proven that the hyperbolic tangent function in the Tanh-SVSF gain removes chattering more effectively than the saturation function from standard SVSF gains. Next, the EK-SVSF-I, UK-SVSF-I, and CK-SVSF-I have roughly the same performance in these figures, which is why these three filters have nearly the same NRMSE in Table 3. For velocity estimation as shown in Figure 5d, the filters presented in [30] and [31] do not estimate the velocity as accurately as other filters due to the following reason. Although the filters from [30] and [31] take advantages of EKF, UKF, and CKF as well as the SVSF in [28], a limitation associated with these approaches is that a full measurement matrix is required, in other words, each state must be measured. To satisfy this requirement, artificial measurements of unmeasured states were created. Since the available measurements are position only, artificial velocity measurements were generated via numerical differentiation of the position as stated earlier. Numerical differentiation results in a higher level of noise in these measurements, leading to less accurate estimation. Next, it is also required to have an artificial measurement for the turn-rate, however, it is not possible to derive an artificial turn-rate measurement using position only, thus, the artificial measurement for turn-rate was set to zero. Since the filters of [30] and [31] utilize the SVSF from [28], the performance of this SVSF algorithm becomes poor in estimating a state that does not have an actual or artificial associated measurement. As a result, in Table 3, the turn-rate estimation provided by these filters has the least accuracy. Since the velocity is dependent on the turn-rate, this causes the velocity to be estimated with the least accuracy. This is why the NRMSEs of these three filters are higher compared to the nonlinear KFs due to poorer velocity and turn-rate estimation.

At 50 s on-wards, as shown in Figures 4d and 5d, when there is model mismatch, the proposed approaches perform better than the filters presented in [40] through taking advantage of the SVSF as well as the EKF, UKF, and CKF. When the computed boundary layer widths are lower than the thresholds, the level of modelling uncertainty is lower,

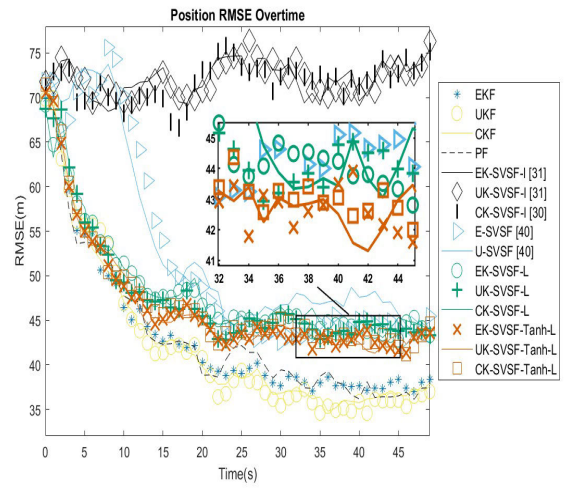
TABLE 3. State Estimation RMSE.

Filter	p_{x_k}	p_{y_k}	v_{x_k}	v_{y_k}	ω_k	NRMSE
EKF	139.963	86.260	47.581	25.069	0.0291	0.3700
UKF	100.310	67.025	43.007	21.119	0.0284	0.3436
CKF	106.871	70.068	43.358	21.577	0.0282	0.3450
PF	1011.1	1122.5	85.507	82.240	0.0390	0.7643
EK-SVSF-I	52.980	50.340	51.278	37.332	0.0570	0.5954
UK-SVSF-I	52.606	50.812	51.168	37.491	0.0570	0.5956
CK-SVSF-I	52.677	50.610	51.087	37.052	0.0570	0.5946
E-SVSF	45.552	42.961	44.588	24.892	0.0313	0.3694
U-SVSF	43.712	42.429	41.697	24.056	0.0308	0.3582
EK-SVSF-L	37.969	36.206	37.401	19.593	0.0279	0.3194
UK-SVSF-L	37.473	36.183	37.186	19.746	0.0278	0.3182
CK-SVSF-L	37.935	36.241	37.152	19.897	0.0278	0.3183
EK-Tanh-SVSF-L	36.821	35.562	36.223	18.363	0.0273	0.3097
UK-Tanh-SVSF-L	36.888	35.537	36.131	18.331	0.0272	0.3093
CK-Tanh-SVSF-L	36.959	35.825	36.028	18.540	0.0272	0.3094

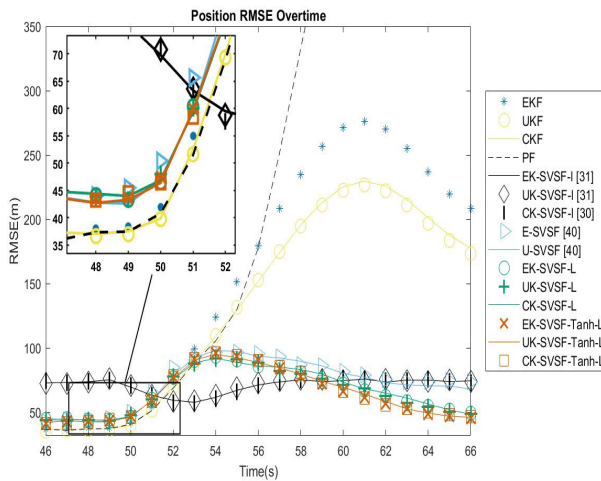
thus, EKF, UKF, and CKF gains are applied. When the widths are higher, the SVSF gains are used to take advantage of the robustness and stability of SVSF. Even though the filters of [40] do apply EKF and UKF features of linearization and sigma points, the SVSF gain is still used to update the states. In Table 3 and Figure 5e, at 50 s on-wards, the proposed filters also outperform the nonlinear KFs and the PF for velocity estimation again due to robustness against modelling error and stability from SVSF's switching gain causing the estimate to converge closer to the true velocity. In Table 3, filters of [30] and [31] provide the least accurate estimates of turn-rate. This also reflects why the velocity is not estimated as accurately compared to other methods in Figure 5d due to the dependence of velocity on turn-rate. However, the proposed SVSF-based methods estimate the turn-rate and velocity more accurately than the filters in [30] and [31]. This is due to employing a reduced-order observer approach to estimate unmeasured states more robustly compared to the filters of [30] and [31]. Therefore, the proposed approaches estimate position and velocity more accurately than other methods, and achieve a lower NRMSE compared to the others. Lastly, the EK-Tanh-SVSF-L, UK-Tanh-SVSF-L, and CK-Tanh-SVSF-L perform better than all filters overall for position and velocity estimation as shown in Table 3. In Figures 4d, 5c, and 5d, once model mismatch is present after 49 s, the EK-Tanh-SVSF-L, UK-Tanh-SVSF-L, and CK-Tanh-SVSF-L estimate the position and velocity the most accurately compared to other filters. For position, as shown in Figure 4d, the filters employing Tanh-SVSF-L perform slightly better than the ones using SVSF-L between 59 s and 67 s. For velocity estimation in Figure 5d, from 58 s to 65 s, the Tanh-SVSF-L-based filters perform slightly better than the ones employing SVSF-L. Also, in Figure 5c, from 53-58 s into the simulation, the filters using Tanh-SVSF-L outperform the filters employing SVSF-L. These filters marginally outperform EK-SVSF-L, UK-SVSF-L, and CK-SVSF-L regarding NRMSE, because they take advantage of the Tanh-SVSF gains proposed in [37]. This allows these methods to suppress chattering more effectively, because in [37], it is proven that replacing the saturation function in



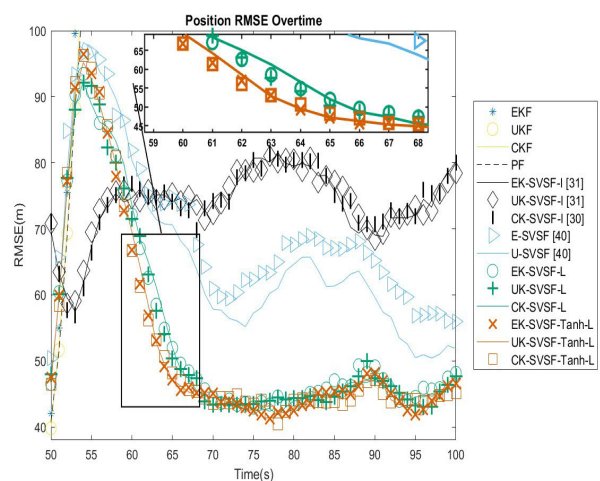
(a) Position RMSE throughout the simulation



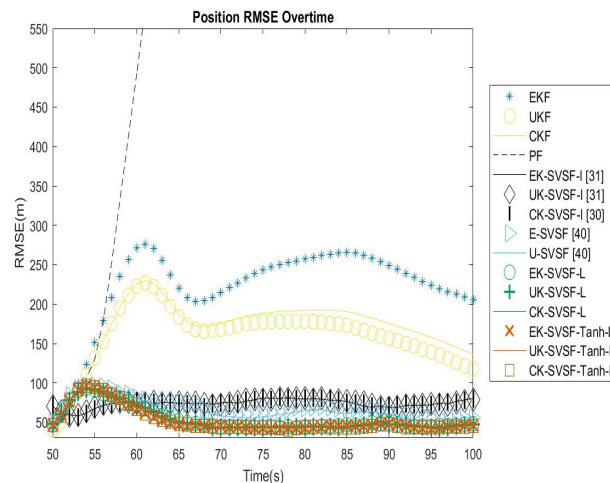
(b) Position RMSE prior to turning in opposite direction



(c) Position RMSE soon before and after turning in the opposite direction

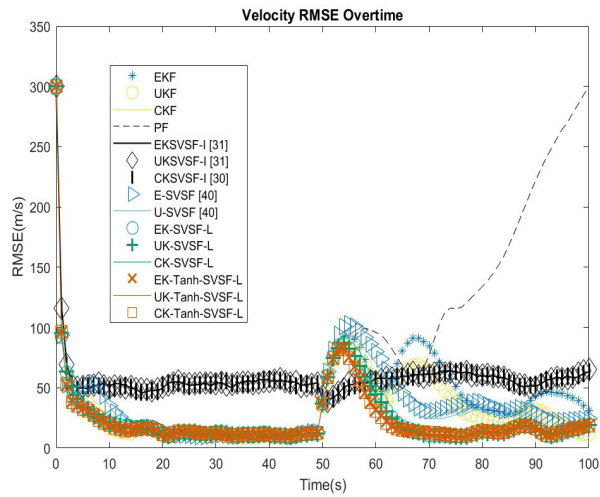


(d) Position RMSE after turning in the opposite direction

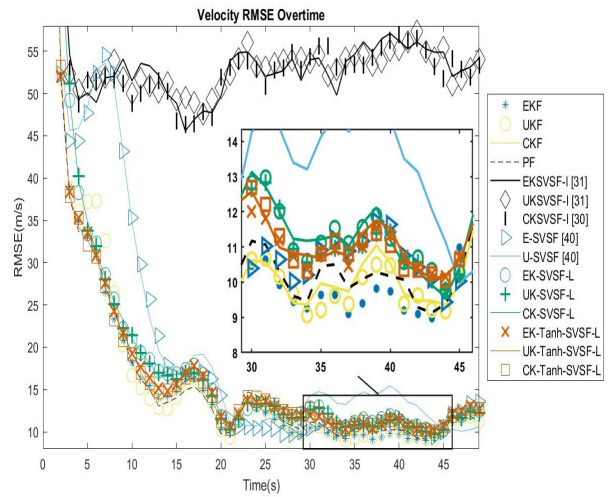


(e) Enlarged view of position RMSE after turning in the opposite direction

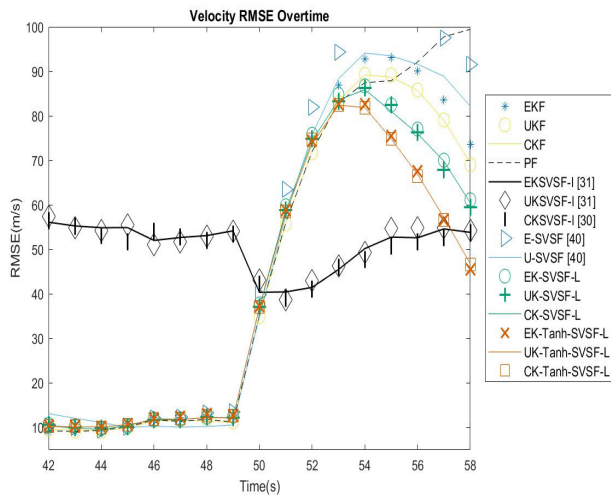
FIGURE 4. Position Estimation RMSE.



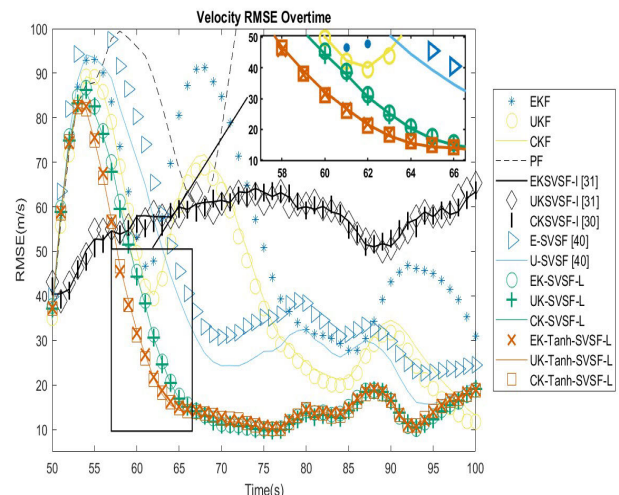
(a) Velocity RMSE though-out the simulation



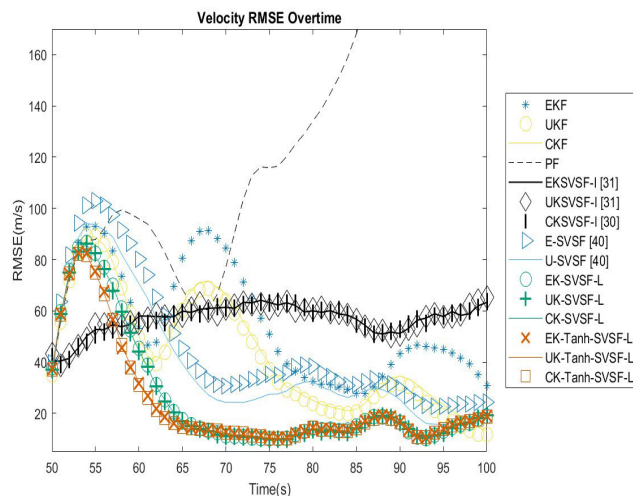
(b) Velocity RMSE before turning in the opposite direction



(c) Velocity RMSE shortly before and after turning in the opposite direction

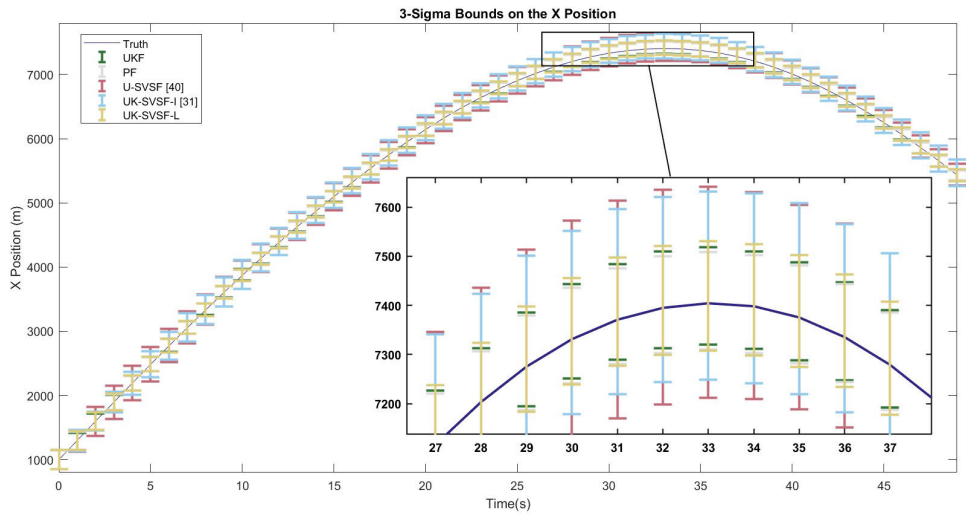


(d) Velocity RMSE after turning in the opposite direction

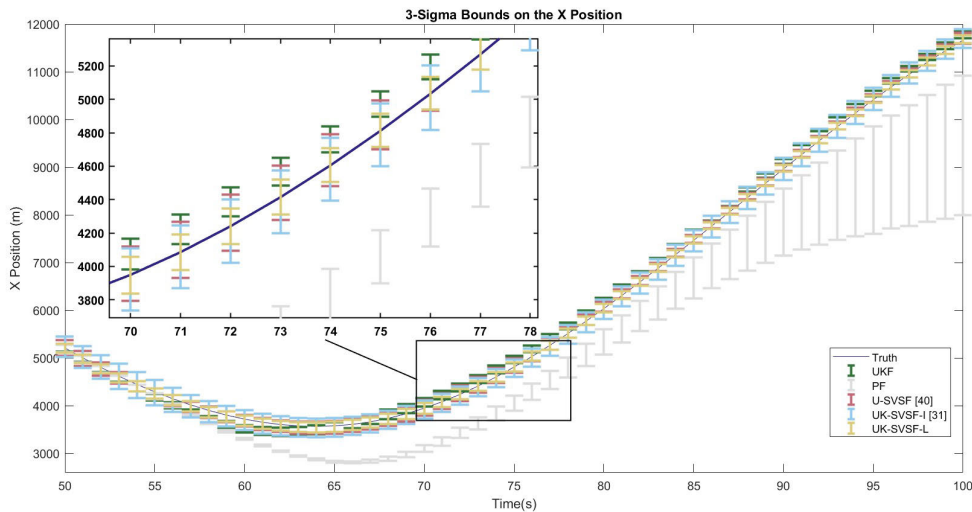


(e) Enlarged view of velocity RMSE after turning in the opposite direction

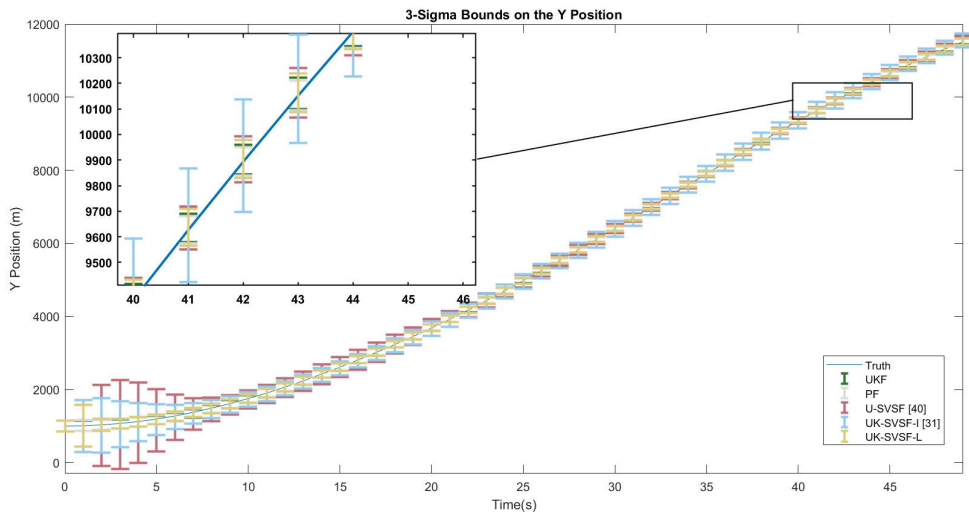
FIGURE 5. Velocity Estimation RMSE.



(a) 3-sigma bounds for the x position before the target turns in the opposite direction

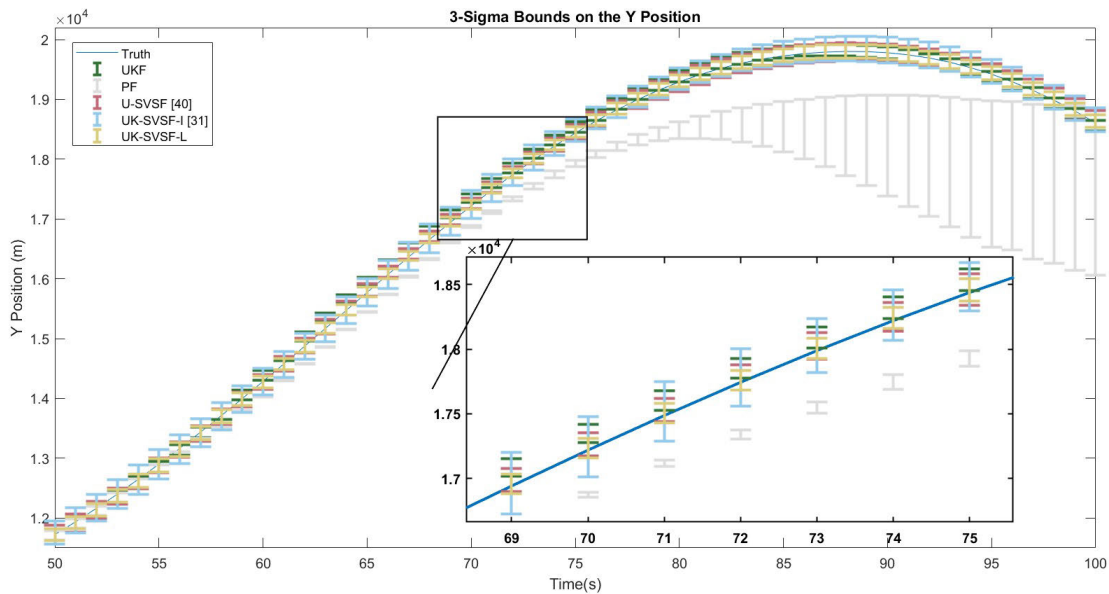


(b) 3-sigma bounds for the x position after the target turns in the opposite direction



(c) 3-sigma bounds for the y position before the target turns in the opposite direction

FIGURE 6. 3-sigma bounds on position.

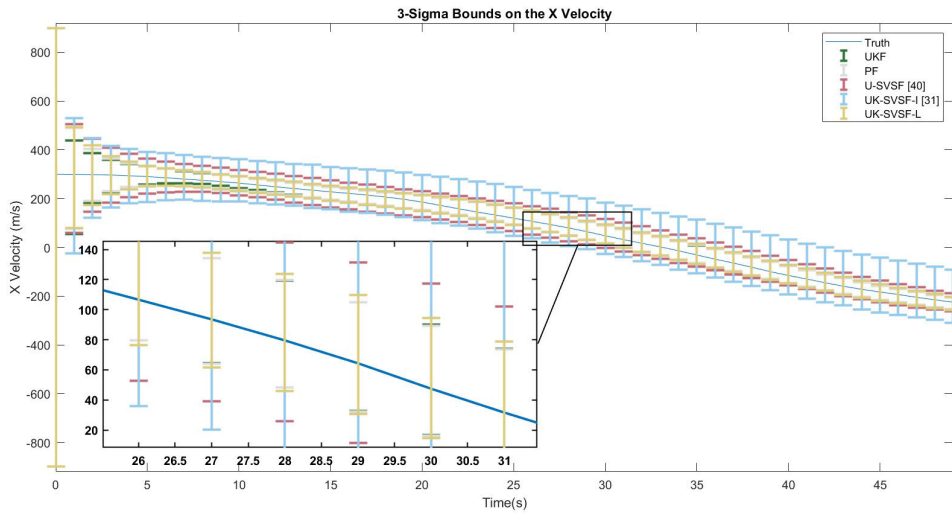
(d) 3-sigma bounds for the y position after the target turns in the opposite direction**FIGURE 6.** (Continued.) 3-sigma bounds on position.

the standard SVSF gain with a hyperbolic tangent function results in greater chattering reduction. This in turn improves the estimation accuracy.

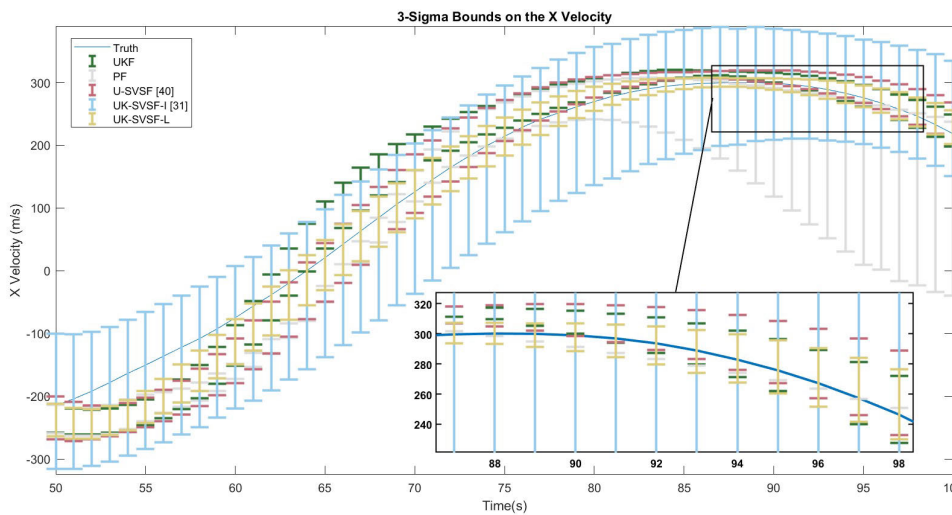
The 3-sigma bounds on the position and velocity are shown in Figures 6 and 7, respectively. Note that to make the comparisons between the bounds for each filter easier to see visually, the bounds are not shown for all filters because based on Table 3, the 6 proposed filters have comparable performance with each other in terms of NRMSE, the UK-SVSF-I achieves nearly the same tracking accuracy as EK-SVSF-I and CK-SVSF-I, E-SVSF's NRMSE is marginally different from U-SVSF, and because CKF's NRMSE is comparable to UKF. Only the results of UKF, PF, UK-SVSF-I, U-SVSF, and UK-SVSF-L are shown.

For the x and y position, it can be observed that in Figures 6a and 6c, the true position is kept within the 3-sigma bounds for all filters before the target turns in the opposite direction at 50 s. Prior to 50 s, for both x and y position, as illustrated in the zoomed in parts, the PF and UKF have smaller gaps between their bounds compared to the SVSFs, which is expected as the filter model is accurate, indicating more accurate state estimates from the UKF and PF compared to the others. Since the bars for the UKF and PF almost overlap with each other in Figures 6a and 6c, the gap length for both filters are almost the same. The gap between the bounds for UK-SVSF-L is slightly larger than UKF because this filter has the ability to apply the UKF when the level of modelling error is lower. Since the filter model is precise before 50s, the BL widths would be smaller and the level of modelling error is expected to be low. Hence, theoretically, it would apply the UKF gains more often, making the gap

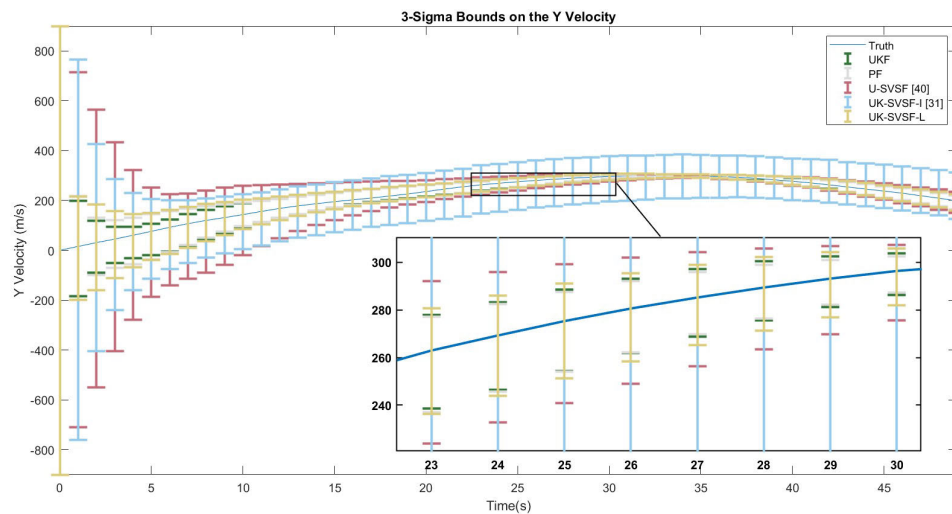
between the bounds slightly larger than the gap for UKF. The U-SVSF only applies SVSF gains, hence, it is not expected to give the best performance when there is no modelling error, making the gap between the bounds larger for this filter in comparison to the PF, UKF, and UK-SVSF-L as shown in the zoomed in parts of Figures 6a and 6c. The UK-SVSF-I can also utilize UKF filtering, but the issue is that it requires artificial measurements of unmeasured states, which increases noise levels as numerical differentiation was applied to obtain velocity measurements. It also requires a turn-rate measurement, which is not possible to derive using position-only measurements as stated earlier, and a limitation associated with filters using SVSF-I is that the SVSF-I has a poor performance in estimating states without an associated real or artificial measurement. Since velocity is a function of the turn-rate, this in turn causes the velocity to be estimated poorly. Hence, this makes the gap larger compared to UKF, PF, and UK-SVSF-L as illustrated in Figures 6a and 6c, which indicates less precise tracking performance. In Figures 6b and 6d, which is when modelling uncertainty is present due to the target turning in the opposite direction, based on the zoomed in parts, it can be seen that the bounds for the UKF do not contain the true position. This is due to the lack of robustness against modelling error for the UKF and because the UKF is less stable. The 3-sigma bounds of the PF do not keep the true position for majority of the time after 49 s because of instability due to an inaccurate model. As shown in Figures 6b and 6d, the gap between the sigma bounds also rises overtime for the PF due to it becoming unstable, hence, the confidence in the position estimate is declining, and this indicates the estimate is becoming less accurate. Whereas,



(a) 3-sigma bounds for the x velocity before the target turns in the opposite direction

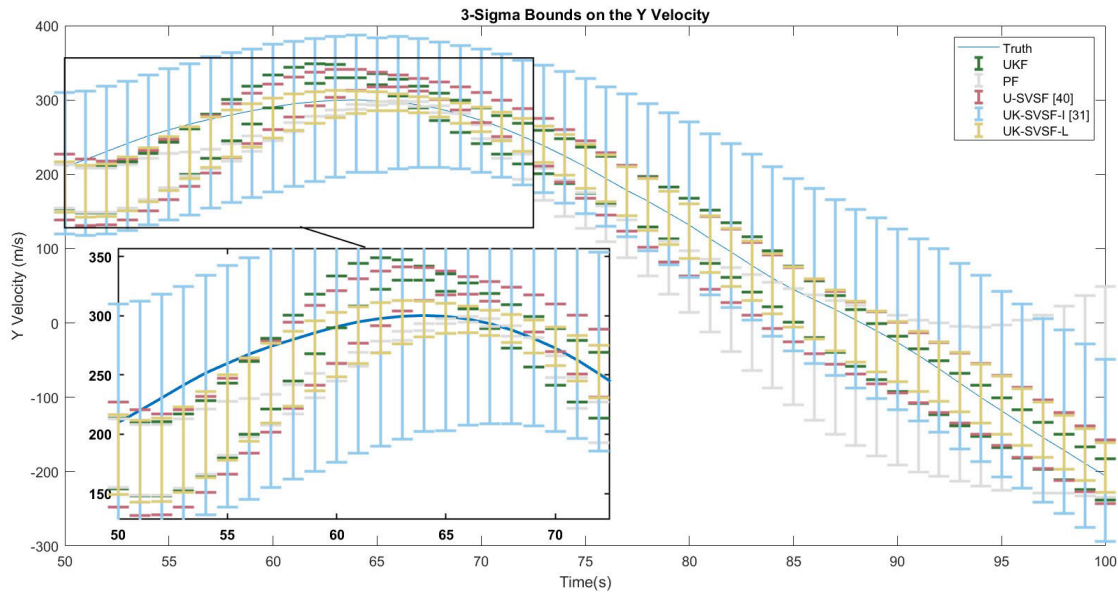


(b) 3-sigma bounds for the x velocity after the target turns in the opposite direction



(c) 3-sigma bounds for the y velocity before the target turns in the opposite direction

FIGURE 7. 3-sigma bounds on velocity.

(d) 3-sigma bounds for the y velocity after the target turns in the opposite direction**FIGURE 7. (Continued.) 3-sigma bounds on velocity.**

based on the zoomed in parts in Figures 6b and 6d, for the SVSFs, the true position is kept within the 3-sigma bounds due to robustness against modelling error and stability.

Next, for the x and y velocity, based on Figures 7a and 7c, which is when no modelling error is present, all filters keep the true velocity within their 3-sigma bounds. Similarly, the gap between the bounds for the UKF and PF are lower compared to the SVSFs since there is no model mismatch before 50 s. The PF and UKF have nearly the same length for their gaps since the bars almost overlap as shown in Figures 7a and 7c. The UK-SVSF-L has the ability to utilize UKF filtering when the level of modelling error is low, which is why the gap for it is slightly larger than UKF as discussed in the previous paragraph. For majority of the time before 50 s, the UK-SVSF-I has a larger gap between the bounds for both x and y velocity in comparison to the PF, UKF, U-SVSF and UK-SVSF-L as shown in Figures 7a and 7c. This is because it uses artificial velocity measurements from numerical differentiation and because it uses a turn-rate of zero as explained earlier, which then causes the velocity and turn-rate to be estimated with the least accuracy. Once, the target turns in the opposite direction, for the PF, based on Figures 7b and 7d, for majority of the time after 50 s, due to instability and lack of robustness, the gap between the bounds is increasing overtime, thus, the confidence in the velocity estimate declines. This indicates the velocity estimate is becoming less precise. For the x velocity, as shown in Figure 7b, between 61-63 s, the UKF keeps the true x velocity within its bounds, afterwards, it goes outside the bounds, and after a while, at 91 s on-wards, as shown in the zoomed in figure, the true velocity is within the bounds. Whereas, for the UK-SVSF-L, at 63 s on-wards, it keeps

the velocity in its bounds. Due to improved robustness and stability, it keeps the true velocity within the bounds for a longer period compared to UKF. Next, for the y velocity, at 50 s on-wards, as shown in Figure 7d, for UKF, from 57-59 s, the true velocity is kept within the bounds, however, between 60-66 s, it is not within the bounds. For UK-SVSF-L, at 57 s and beyond, the true velocity is kept within the 3-sigma bounds. Hence, in this case, it also keeps the true velocity within the bounds for a longer time due to stability and robustness from the SVSF gain.

IV. CONCLUSION

In this paper, a general framework is formed that puts a subset of existing SVSF methods under one umbrella. More specifically, a new strategy to combine SVSF with other state-of-the-art nonlinear filters is proposed. This results in a set of six new combined SVSF filtering strategies, the derivation and simulation results of all were presented. The Luenberger SVSF (SVSF-L) and the Luenberger Tanh-SVSF (Tanh-SVSF-L) were combined with EKF, UKF, and CKF. These filters are abbreviated as EK-SVSF-L, UK-SVSF-L, CK-SVSF-L, EK-Tanh-SVSF-L, UK-Tanh-SVSF-L, and CK-Tanh-SVSF-L. Since existing SVSF strategies can be discovered as special cases of the proposed filters, this allows the framework to put existing strategies under one umbrella. Moreover, another contribution is that the limitations of these filters are relaxed. The proposed filters extend linear SVSF algorithms, called Generalized Variable Boundary Layer-Smooth Variable Structure Filter (GVBL-SVSF) and Nonlinear Variable Boundary Layer-Smooth Variable Structure Filter (NVBL-SVSF) to non-linear systems, where the number of measured states (outputs) is less than the number

of states without having to generate artificial measurements. These strategies also extend the domain of applicability of filtering algorithms presented in [30] and [31] by relaxing the requirement of having a square measurement matrix, since in many applications not all states are measurable and it is not always possible to create an artificial measurement of each state as shown in this paper. Measuring all states may require additional sensors, which may increase the cost of system design, thus, relaxing the requirement of a full measurement matrix reduces the system cost. A subset of existing SVSF strategies can be viewed as special cases of the proposed framework.

All six filters were evaluated to track a maneuvering target. It was demonstrated that the new SVSF approaches outperform the EKF, UKF, CKF, and PF due to their stability and robustness against modelling error when using models that are not representative of the target's true motion. The proposed methods also estimate the target's position and velocity more accurately compared to some existing non-linear SVSF strategies. Moreover, under modelling uncertainty, the proposed filters that employ Tanh-SVSF perform the best in terms of position and velocity estimation accuracy because the Tanh-SVSF's gains suppress the chattering more effectively compared to standard SVSF gains.

REFERENCES

- [1] Y. Ho and R. Lee, "A Bayesian approach to problems in stochastic estimation and control," *IEEE Trans. Autom. Control*, vol. AC-9, no. 4, pp. 333–339, Oct. 1964, doi: [10.1109/TAC.1964.1105763](https://doi.org/10.1109/TAC.1964.1105763).
- [2] R. E. Kalman, "A new approach to linear filtering and prediction problems," *J. Basic Eng.*, vol. 82, no. 1, pp. 35–45, Mar. 1960, doi: [10.1115/1.3662552](https://doi.org/10.1115/1.3662552).
- [3] M. S. Grewal and A. P. Andrews, *Kalman filtering: Theory and Practice with MATLAB*. Hoboken, NJ, USA: Wiley, 2008.
- [4] Y. Bar-Shalom, X. R. Li, and T. Kirubarajan, *Estimation With Applications to Tracking and Navigation: Theory Algorithms and Software*. New York, NY, USA: Wiley, 2001.
- [5] P. Setoodeh, S. Habibi, and S. Haykin, *Nonlinear Filters: Theory and Applications*. Hoboken, NJ, USA: Wiley, 2022.
- [6] S. J. Julier and J. K. Uhlmann, "New extension of the Kalman filter to nonlinear systems," *Proc. SPIE*, vol. 3068, pp. 182–193 Jul. 1997, doi: [10.1117/12.280797](https://doi.org/10.1117/12.280797).
- [7] E. A. Wan and R. van der Merwe, "The unscented Kalman filter for nonlinear estimation," in *Proc. IEEE Adapt. Syst. Signal Process., Commun., Control Symp. (AS-SPCC)*, Lake Louise, AB, Canada, Oct. 2000, pp. 153–158, doi: [10.1109/ASSPCC.2000.882463](https://doi.org/10.1109/ASSPCC.2000.882463).
- [8] Y. Bar-Shalom and X. R. Li, *Multitarget-Multisensor Tracking: Principles and Techniques*. Storrs, CT, USA: YBS Publishing, 1995.
- [9] I. Hwang, H. Balakrishnan, K. Roy, and C. Tomlin, "Multiple-target tracking and identity management in clutter, with application to aircraft tracking," in *Proc. Amer. Control Conf.*, Boston, MA, USA, 2004, pp. 3422–3428, doi: [10.23919/ACC.2004.1384439](https://doi.org/10.23919/ACC.2004.1384439).
- [10] S. H. Rezaatofghi, S. Gould, B. T. Vo, B.-N. Vo, K. Mele, and R. Hartley, "Multi-target tracking with time-varying clutter rate and detection profile: Application to time-lapse cell microscopy sequences," *IEEE Trans. Med. Imag.*, vol. 34, no. 6, pp. 1336–1348, Jun. 2015, doi: [10.1109/TMI.2015.2390647](https://doi.org/10.1109/TMI.2015.2390647).
- [11] D. Schulz, W. Burgard, D. Fox, and A. B. Cremers, "Tracking multiple moving objects with a mobile robot," in *Proc. IEEE Comput. Soc. Conf. Comput. Vis. Pattern Recognit. CVPR*, Kauai, HI, USA, Dec. 2001, pp. I-371–I-377, doi: [10.1109/CVPR.2001.990499](https://doi.org/10.1109/CVPR.2001.990499).
- [12] B. Kim, K. Yi, H.-J. Yoo, H.-J. Chong, and B. Ko, "An IMM/EKF approach for enhanced multitarget state estimation for application to integrated risk management system," *IEEE Trans. Veh. Technol.*, vol. 64, no. 3, pp. 876–889, Mar. 2015, doi: [10.1109/TVT.2014.2329497](https://doi.org/10.1109/TVT.2014.2329497).
- [13] J. Zhang, W. Xiao, B. Coifman, and J. P. Mills, "Vehicle tracking and speed estimation from roadside LIDAR," *IEEE J. Sel. Topics Appl. Earth Observ. Remote Sens.*, vol. 13, pp. 5597–5608, 2020, doi: [10.1109/JSTARS.2020.3024921](https://doi.org/10.1109/JSTARS.2020.3024921).
- [14] C. Chen, L. Fragonara, and A. Tsourdos, "3D car tracking using fused data in traffic scenes for autonomous vehicle," in *Proc. 5th Int. Conf. Vehicle Technol. Intell. Transp. Syst.*, vol. 1, Crete, Greece, Jan. 2019, pp. 312–318, doi: [10.5220/0007674203120318](https://doi.org/10.5220/0007674203120318).
- [15] L. Xie, Y. C. Soh, and C. E. de Souza, "Robust Kalman filtering for uncertain discrete-time systems," *IEEE Trans. Autom. Control*, vol. 39, no. 6, pp. 1310–1314, Jun. 1994, doi: [10.1109/9.293203](https://doi.org/10.1109/9.293203).
- [16] B. Hassibi and T. Kailath, "H_∞ adaptive filtering," in *Proc. Int. Conf. Acoust., Speech, Signal Process.*, vol. 2, Detroit, MI, USA, May 1995, pp. 949–952, doi: [10.1109/ICASSP.1995.480332](https://doi.org/10.1109/ICASSP.1995.480332).
- [17] S. Habibi, "The smooth variable structure filter," *Proc. IEEE*, vol. 95, no. 5, pp. 1026–1059, May 2007, doi: [10.1109/JPROC.2007.893255](https://doi.org/10.1109/JPROC.2007.893255).
- [18] R. Ahmed, M. El Sayed, S. A. Gadsden, J. Tjong, and S. Habibi, "Artificial neural network training utilizing the smooth variable structure filter estimation strategy," *Neural Comput. Appl.*, vol. 27, no. 3, pp. 537–548, Apr. 2016, doi: [10.1007/s00521-015-1875-2](https://doi.org/10.1007/s00521-015-1875-2).
- [19] S. Rahimifard, R. Ahmed, and S. Habibi, "Interacting multiple model strategy for electric vehicle batteries state of charge/health/power estimation," *IEEE Access*, vol. 9, pp. 109875–109888, 2021, doi: [10.1109/ACCESS.2021.3102607](https://doi.org/10.1109/ACCESS.2021.3102607).
- [20] M. AlShabi and A. Elnady, "Recursive smooth variable structure filter for estimation processes in direct power control scheme under balanced and unbalanced power grid," *IEEE Syst. J.*, vol. 14, no. 1, pp. 971–982, Mar. 2020, doi: [10.1109/JSYST.2019.2919792](https://doi.org/10.1109/JSYST.2019.2919792).
- [21] R. Ahmed, M. El Sayed, S. A. Gadsden, J. Tjong, and S. Habibi, "Automotive internal-combustion-engine fault detection and classification using artificial neural network techniques," *IEEE Trans. Veh. Technol.*, vol. 64, no. 1, pp. 21–33, Jan. 2015, doi: [10.1109/TVT.2014.2317736](https://doi.org/10.1109/TVT.2014.2317736).
- [22] M. Attari, Z. Luo, and S. Habibi, "An SVSF-based generalized robust strategy for target tracking in clutter," *IEEE Trans. Intell. Transp. Syst.*, vol. 17, no. 5, pp. 1381–1392, May 2016, doi: [10.1109/TITS.2015.2504331](https://doi.org/10.1109/TITS.2015.2504331).
- [23] F. Demim, S. Benmansour, N. Abdelkrim, A. Rouigeb, M. Hamerlain, and A. Bazoula, "Simultaneous localisation and mapping for autonomous underwater vehicle using a combined smooth variable structure filter and extended Kalman filter," *J. Experim. Theor. Artif. Intell.*, vol. 34, no. 4, pp. 621–650, Jul. 2022, doi: [10.1080/0952813X.2021.1908430](https://doi.org/10.1080/0952813X.2021.1908430).
- [24] J. Goodman, J. Kim, A. S. Lee, S. A. Gadsden, and M. Al-Shabi, "A variable structure-based estimation strategy applied to an RRR robot system," *J. Robot., Netw. Artif. Life*, vol. 4, no. 2, p. 142, 2017, doi: [10.2991/jrnal.2017.4.2.8](https://doi.org/10.2991/jrnal.2017.4.2.8).
- [25] L. Cao, Y. Chen, Z. Zhang, H. Li, and A. K. Misra, "Predictive smooth variable structure filter for attitude synchronization estimation during satellite formation flying," *IEEE Trans. Aerosp. Electron. Syst.*, vol. 53, no. 3, pp. 1375–1383, Jun. 2017, doi: [10.1109/TAES.2017.2671118](https://doi.org/10.1109/TAES.2017.2671118).
- [26] S. Akhtar and S. Habibi, "The interacting multiple model smooth variable structure filter for trajectory prediction," *IEEE Trans. Intell. Transp. Syst.*, vol. 24, no. 9, pp. 9217–9239, Sep. 2023, doi: [10.1109/TITS.2023.3271295](https://doi.org/10.1109/TITS.2023.3271295).
- [27] M. Avzayesh, M. Abdel-Hafez, M. AlShabi, and S. A. Gadsden, "The smooth variable structure filter: A comprehensive review," *Digit. Signal Process.*, vol. 110, Mar. 2021, Art. no. 102912, doi: [10.1016/j.dsp.2020.102912](https://doi.org/10.1016/j.dsp.2020.102912).
- [28] S. A. Gadsden and S. R. Habibi, "A new form of the smooth variable structure filter with a covariance derivation," in *Proc. 49th IEEE Conf. Decis. Control (CDC)*, Atlanta, GA, USA, Dec. 2010, pp. 7389–7394, doi: [10.1109/CDC.2010.5717397](https://doi.org/10.1109/CDC.2010.5717397).
- [29] S. A. Gadsden and S. R. Habibi, "A new robust filtering strategy for linear systems," *J. Dyn. Syst., Meas., Control*, vol. 135, no. 1, Jan. 2013, Art. no. 014503, doi: [10.1115/1.4006628](https://doi.org/10.1115/1.4006628).
- [30] S. A. Gadsden, M. Al-Shabi, I. Arasaratnam, and S. R. Habibi, "Combined cubature Kalman and smooth variable structure filtering: A robust nonlinear estimation strategy," *Signal Process.*, vol. 96, pp. 290–299, Mar. 2014, doi: [10.1016/j.sigpro.2013.08.015](https://doi.org/10.1016/j.sigpro.2013.08.015).
- [31] S. A. Gadsden, S. Habibi, and T. Kirubarajan, "Kalman and smooth variable structure filters for robust estimation," *IEEE Trans. Aerosp. Electron. Syst.*, vol. 50, no. 2, pp. 1038–1050, Apr. 2014, doi: [10.1109/TAES.2014.110768](https://doi.org/10.1109/TAES.2014.110768).

- [32] S. A. Gadsden, D. Dunne, S. R. Habibi, and T. Kirubarajan, "Combined particle and smooth variable structure filtering for nonlinear estimation problems," in *Proc. 14th Int. Conf. Inf. Fusion*, Chicago, IL, USA, Jul. 2011, pp. 1–8.
- [33] S. A. Gadsden, S. R. Habibi, and T. Kirubarajan, "A novel interacting multiple model method for nonlinear target tracking," in *Proc. 13th Int. Conf. Inf. Fusion*, Edinburgh, U.K., Jul. 2010, pp. 1–8, doi: [10.1109/ICIF.2010.5712021](https://doi.org/10.1109/ICIF.2010.5712021).
- [34] M. Attari, S. Habibi, and S. A. Gadsden, "Target tracking formulation of the SVSF with data association techniques," *IEEE Trans. Aerosp. Electron. Syst.*, vol. 53, no. 1, pp. 12–25, Feb. 2017, doi: [10.1109/TAES.2017.2649138](https://doi.org/10.1109/TAES.2017.2649138).
- [35] S. Gadsden, M. Al-Shabi, and T. Kirubarajan, "Square-root formulation of the SVSF with applications to nonlinear target tracking problems," *Proc. SPIE*, vol. 9474, May 2015, pp. 54–65, doi: [10.1117/12.2177226](https://doi.org/10.1117/12.2177226).
- [36] H. H. Afshari, S. A. Gadsden, and S. Habibi, "A nonlinear second-order filtering strategy for state estimation of uncertain systems," *Signal Process.*, vol. 155, pp. 182–192, Feb. 2019, doi: [10.1016/j.sigpro.2018.09.036](https://doi.org/10.1016/j.sigpro.2018.09.036).
- [37] Y. Li, G. Li, Y. Liu, X.-P. Zhang, and Y. He, "A novel smooth variable structure filter for target tracking under model uncertainty," *IEEE Trans. Intell. Transp. Syst.*, vol. 23, no. 6, pp. 5823–5839, Jun. 2022, doi: [10.1109/TITS.2021.3058806](https://doi.org/10.1109/TITS.2021.3058806).
- [38] Y. Li, G. Li, Y. Liu, X.-P. Zhang, and Y. He, "A hybrid SVSF algorithm for automotive radar tracking," *IEEE Trans. Intell. Transp. Syst.*, vol. 23, no. 9, pp. 15028–15042, Sep. 2022, doi: [10.1109/TITS.2021.3136170](https://doi.org/10.1109/TITS.2021.3136170).
- [39] I. Arasaratnam and S. Haykin, "Cubature Kalman filters," *IEEE Trans. Autom. Control*, vol. 54, no. 6, pp. 1254–1269, Jun. 2009, doi: [10.1109/TAC.2009.2019800](https://doi.org/10.1109/TAC.2009.2019800).
- [40] Y. Chen, G. Wang, L. Xu, and B. Yan, "A new strategy of smooth variable structure filter to estimate unmeasured states in target tracking," *Digit. Signal Process.*, vol. 123, Apr. 2022, Art. no. 103428, doi: [10.1016/j.dsp.2022.103428](https://doi.org/10.1016/j.dsp.2022.103428).
- [41] K. Deb, A. Pratap, S. Agarwal, and T. Meyarivan, "A fast and elitist multiobjective genetic algorithm: NSGA-II," *IEEE Trans. Evol. Comput.*, vol. 6, no. 2, pp. 182–197, Apr. 2002, doi: [10.1109/4235.996017](https://doi.org/10.1109/4235.996017).
- [42] M. A. Al-Shabi, "The general Toeplitz/observability smooth variable structure filter," Ph.D. dissertation, Dept. Mech. Eng., McMaster Univ., Hamilton, ON, Canada, 2011.



SALMAN AKHTAR received the B.Eng. degree in electrical engineering from McMaster University, Hamilton, ON, Canada, in 2019, where he is currently pursuing the Ph.D. degree in mechanical engineering. During the bachelor's degree, as a Co-Op Student, he was with Defence Research and Development Canada (DRDC), where he developed algorithms to de-interleave and identify cognitive radar signals using signal processing and machine learning techniques. His current research interests include state and parameter estimation theory, systems and control theory, signal processing, multi-target tracking, sensor fusion, autonomous driving, and machine learning.



PEYMAN SETOODEH (Senior Member, IEEE) received the B.Sc. and M.Sc. degrees (Hons.) in electrical engineering from Shiraz University, and the Ph.D. degree in computational engineering and science from McMaster University. He is currently with the Centre for Mechatronics and Hybrid Technologies (CMHT), McMaster University. He was the Harrison McCain Visiting Professor with the Marine Additive Manufacturing Centre of Excellence (MAMCE), University of New Brunswick; and an Associate Professor with the School of Electrical and Computer Engineering, Shiraz University. Previously, he was a Senior Research Engineer with the Huawei Noah's Ark Laboratory; and a Lecturer with the Department of Electrical and Computer Engineering, McMaster University. He was a recipient of the Monbukagakusho Scholarship from the Ministry of Education, Culture, Sports, Science, and Technology, Japan. He has coauthored two books, such as *Fundamentals of Cognitive Radio and Nonlinear Filters: Theory and Applications*. He is a coauthor of a paper on cognitive control, which was featured as the cover story of the PROCEEDINGS OF THE IEEE in the December issue of the centennial year. His research interests include cognitive systems, artificial intelligence, quantum control, and nonlinear estimation.



RYAN AHMED received the M.A.Sc. degree from McMaster University, focusing on artificial intelligence and fault detection, the M.B.A. degree in finance from the DeGroote School of Business, and the Ph.D. degree in engineering, focusing on battery modeling, state of charge, and state of health estimation. He is an Assistant Professor with the Department of Mechanical Engineering, McMaster University. Prior to joining McMaster University, he held several senior engineering positions globally with General Motors, Fiat-Chrysler, and Samsung. He taught several courses on science, technology, engineering, and mathematics to over 340,000 students from 160 countries with more than 29,000 five-star reviews and an overall rating of 4.5/5. He is the principal author and the coauthor of over 35 journal and conference publications. His research interests include smart systems, artificial intelligence, energy storage devices, autonomous systems, and electric powertrains. He was a co-recipient of two Best Papers Awards at the IEEE TRANSACTIONS ON INDUSTRIAL ELECTRONICS, in 2018; and at the IEEE Transportation Electrification Conference and Expo (ITEC 2012), Detroit, MI, USA. He is a Stanford Certified Project Manager (SCPM) and a Certified Professional Engineer (P.Eng.) in Ontario. He was the Program Co-Chair of the 2017 IEEE Transportation and Electrification Conference (iTEC'17), Chicago, IL, USA.



SAEID HABIBI (Member, IEEE) received the Ph.D. degree in control engineering from the University of Cambridge, U.K., in 1990. He is a Tier I Canada Research Chair and a Full Professor with the Department of Mechanical Engineering, McMaster University. He is the Founder and the Director of the Centre for Mechatronics and Hybrid Technologies (CMHT). CMHT has created one of the most advanced and best equipped automotive research laboratories in Canada and internationally, specializing in predictive algorithms, tracking, prognostics, and diagnostics. CMHT currently supports a number of large projects and being a resource to automotive companies and start-ups. CMHT research is supported by industry and by funding from Ontario Research Fund Research Excellence Awards and NSERC. He was the Chair of the Department of Mechanical Engineering, from 2008 to 2013. His academic background includes research into artificial intelligence, intelligent control, state and parameter estimation, fault diagnosis, and prediction. He has published over 200 peer-reviewed papers. He is a fellow of the American Society of Mechanical Engineers (ASME) and the Canadian Society of Mechanical Engineers (CSME).

...